Title

Revising the dynamic energy budget theory with a new reserve mobilization rule and three example applications to bacterial growth

Authors

Tang, Jinyun

Riley, William J

Publication Date

2023-03-01

DOI

10.1016/j.soilbio.2023.108954

Soil Biology and Biochemistry 178 (2023) 108954

Contents lists available at ScienceDirect

Soil Biology and Biochemistry

journal homepage: www.elsevier.com/locate/soilbio

Revising the dynamic energy budget theory with a new reserve mobilization rule and three example applications to bacterial growth

Jinyun Tang *, William J. Riley

Earth and Environmental Sciences Area, Lawrence Berkeley National Laboratory, Berkeley, CA, USA

ARTICLE INFO

Keywords:
Dynamic energy budget theory
Equilibrium chemistry approximation kinetics
Substrate and carbon use efficiency
Substrate uptake
Maintenance respiration
Maximum growth rate
Thermodynamics

ABSTRACT

Dynamic energy budget (DEB) theory has been applied to model a wide range of organisms, including microbes. In the standard DEB model, biomass is partitioned into reserve and structural compartments, where reserve biomass is mobilized in a pseudolinear manner (while the reserve biomass density, defined as the ratio between reserve and structural biomass, decays linearly) to drive maintenance and the growth of structural biomass (and extracellular enzyme production if it is considered). However, the linear dynamics of the reserve biomass density makes the standard DEB model incapable of explaining the slowdown of microbial growth at high reserve density that is caused by macromolecular crowding effect which reduces biochemical reaction rates (a typical situation occurs when microbes are experiencing severe moisture stress) and is inconsistent with the observation that intracellular enzymatic reactions generally follow non-linear kinetics. By partitioning biomass into reserve, kinetic, and structural compartments, we show here that the Equilibrium Chemistry Approximation (ECA) kinetics can be used to represent enzymatically catalyzed reserve biomass mobilization that can then drive the kinetic and structural biomass synthesis. This revised DEB model better represents the tradeoff in ribosome allocation for structural growth and internal enzyme production, is structurally compatible with metabolic models of cell individuals, and includes the standard DEB model and the popular compromise model as special cases for representing population growth. We then applied the revised DEB model to interpret components of bacterial respiration, their dependence on substrate availability, and emergent microbial carbon use efficiency dynamics for an exponentially growing population. We found that the revised DEB model enables a better understanding of bacterial substrates use (carbon in our examples) than that can be derived from a few other models in the literature. In particular, the revised DEB model explains why carbon use efficiency may first increase, then plateau, and finally decrease with growth rate (and substrate uptake rate), as a function of proteomics. Additionally, the revised DEB model explains why the kinetic biomass compartment needs to be divided to reasonably incorporate proteomic control of microbial growth.

1. Introduction

Biological growth is a central theme in many biogeochemical modeling problems. Taking soil carbon dynamics as an example, microbes produce enzymes to harvest Gibbs free energy and synthesize new biomass, meanwhile transforming organic carbon from plant and animal residues into stabilized forms that better integrate with the mineral soil, and release mineral nutrients to support plant growth. Therefore, without microbial growth there would be no recycling of carbon and nutrients, and no biosphere.

A variety of models have been proposed over the past decades to model microbial population growth dynamics. From simple to complex, these include the Monod model (Monod, 1949), the Pirt model (Pirt, 1965, 1982), van Bodegom model (van Bodegom, 2007), the compromise model (Beeftink et al., 1990; Wang and Post, 2012), the cybernetic model (Song and Ramkrishna, 2011), and the dynamic energy budget (DEB) model (Kooijman, 2009). Among them, the DEB model has also been applied to plants and animals (including both individuals and populations), and is compatible with thermodynamics, an essential feature to resolve the tradeoff between growth rate (or substrate uptake rate) and growth yield (Calabrese et al., 2021). Thus, the DEB model is a robust framework for developing a unified theory and model for biological growth.

The main features of a DEB model are that it (1) delineates the

* Corresponding author.
E-mail address: jinyuntang@lbl.gov (J. Tang).

https://doi.org/10.1016/j.soilbio.2023.108954
Received 20 September 2022; Received in revised form 4 January 2023; Accepted 8 January 2023
Available online 10 January 2023

biomass of an organism into structural and reserve compartments; (2) connects the two compartments through the mobilization dynamics of reserve biomass; and (3) represents organism interactions with the environment through the creation of reserve biomass from assimilated external substrates. These features allow an organisms represented by a DEB model to be resilient with respect to fluctuations in environmental conditions (e.g., continued growth after a pause of external substrate supply, which is very typical for animals who feed infrequently), and have shown success in various contexts (Kooijman, 2009). However, we show here that the reserve mobilization dynamics of the standard DEB model prevents it from being consistently derived from enzyme kinetics, so that a logically coherent scaling from a single enzymatic reaction to overall biomass growth cannot be established. We remedy this shortcoming with the Equilibrium Chemistry Approximation kinetics, leading to a revised DEB model that is logically coherent with the law of mass action (for chemical reactions that can be derived from Newtonian statistical mechanics (Pauli, 1973; Hill, 1987)), flux balance analysis (for microbial individuals (Labhsetwar et al., 2017)), and phenological models such as the Monod model.

In the following, we first present the theoretical development on why the standard DEB (sDEB) model needs to be improved, and then how the ECA kinetics can be applied to derive a revised DEB (rDEB) model. Next, we compare the sDEB model, rDEB model, and some other empirically based models with three example applications. Finally, we discuss the potential for further improvement of the rDEB model to obtain a scaling consistent modelling framework of microbial growth.

2. Theory

In this section, we first give a brief description of the sDEB model, focusing on its underlying principles and limitations (section 2.1). Then we propose strategies to resolve those limitations (section 2.2), leading to the rDEB model (section 2.3), the major contribution of this theoretical study.

We note that a full list of symbols can be found in the nomenclature table (Table A). Throughout this work: (1) "specific" variables are normalized by structural biomass, and (2) variables subscripted with "*s*" and "*r*" are for the sDEB and rDEB models, respectively. Variables without subscript "*r*" or "*s*" are not specific to either the sDEB or rDEB model.

2.1. The standard DEB model

In the sDEB model, biomass is partitioned into reserve and structural components (Fig. 1a). Reserve biomass is mobilized to support maintenance and growth of structural biomass (and for eukaryotes, mobilized reserve biomass is also used to fuel maturation (Kooijman, 2009)). The reserve dynamics are formulated according to two principles: (1) if the environmental substrate concentration does not change, then reserve density (defined as the ratio between reserve and structural biomass) becomes constant even when growth (measured as increase in structural biomass) continues; and (2) partitioning reserve biomass into sub-components or merging reserve biomass sub-components does not change the growth dynamics. Principle (2) is also called the partition

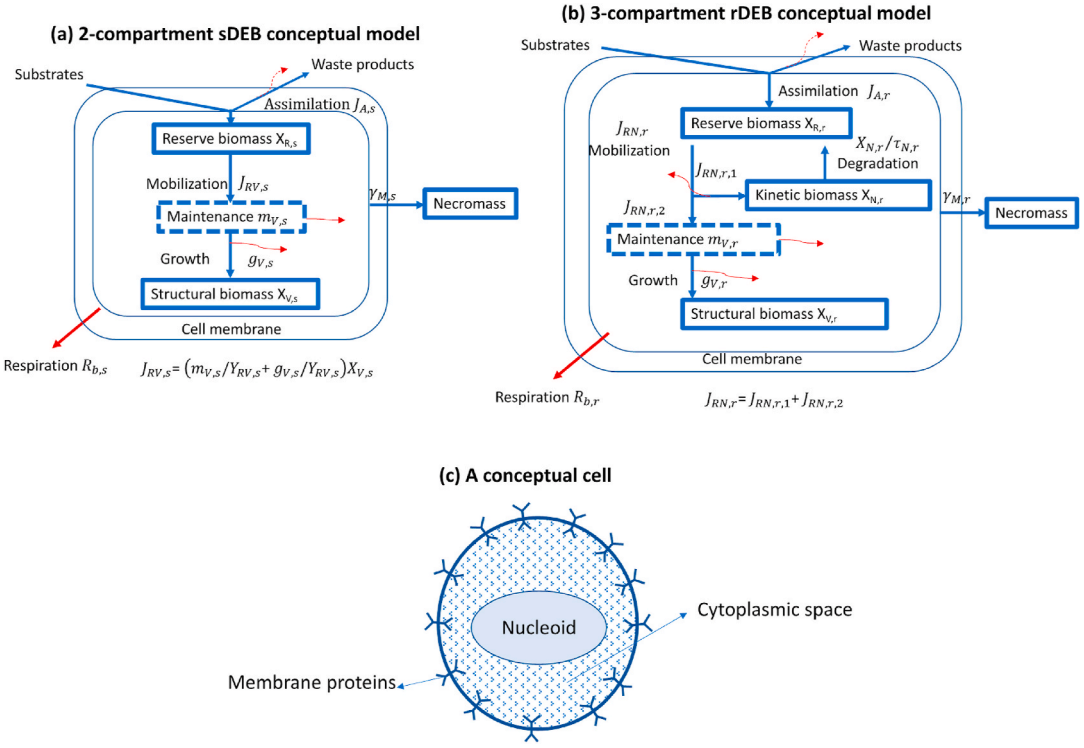

Fig. 1. (a) In the sDEB model, mobilized reserve biomass ($J_{RV,s}$) is first used for maintenance respiration ($m_{V,s}$), and the remaining flux ($J_{RV,s} - m_{V,s}X_{V,s}/Y_{RV,s}$) drives structural biomass growth ($g_{V,s}X_{V,s}/Y_{RV,s}$). Waste products are produced during substrate assimilation and reserve biomass mobilization. Necromass is produced from mortality. Total respiration ($R_{b,s}$, thick solid red line) includes contributions from substrate assimilation (thin dashed red line), maintenance and cost for constructing structural biomass (thin solid red lines). (b) In the rDEB model, substrates are assimilated into reserve biomass (made up of storage compounds and various metabolites), which is then mobilized by kinetic biomass (constituted by various RNAs, ribosomes, and other anabolic and catabolic enzymes) to produce new kinetic biomass ($J_{RN,1}$; including extracellular enzymes) and support maintenance and growth of structural biomass ($J_{RN,2}$; DNA, structural proteins, membranes, etc.). Degraded kinetic biomass is recycled to reserve biomass with turnover time $\tau_{N,r}$. Waste products and necromass are similarly defined as for the sDEB model. Total respiration ($R_{b,r}$ indicated by the thick solid red line) includes contributions from substrate assimilation (thin dashed red line), maintenance, and cost for constructing kinetic and structural biomass (indicated by thin solid red lines). (c) Conceptual spatial structure of a prokaryotic cell. Reserve and kinetic biomass are distributed in the cytoplasmic space that is protected by the structural biomass. Membrane proteins are used for taking up substrates from the environment. Eukaryotes can be conceptualized as a cluster of prokaryotic cells. When applied to a population of cells, the above schematics represent the average state of the whole population.

principle, making the sDEB model align with the observation that reserve dynamics were maintained during evolution from unicellular to multicellular organisms. With this partition principle, the sDEB model is scaling consistent from unicellular to multicellular organisms, and from an individual cell to a population of cells. We note that, in the standard DEB theory, principle (2) can be derived from principle (1) and the strong homeostasis assumption that both structural and reserve biomass are of fixed elemental stoichiometry (but the overall biomass has fluctuating stoichiometry accompanying the change of reserve density; Kooijman, 2009). These two principles lead to the following reserve dynamics for the sDEB model:

$$\frac{dx_{R,s}}{dt} = j_{A,s} - \kappa_s x_{R,s}, \tag{1}$$

where $x_{R,s} = X_{R,s}/X_{V,s}$ is the reserve density, a ratio between reserve biomass $X_{R,s}$ (gC m^{-3}) and structural biomass $X_{V,s}$ (gC m^{-3}); $j_{A,s}$ (s^{-1}) is specific production rate of reserve biomass constructed from substrate assimilation; and κ_s (s^{-1}) is specific reserve mobilization rate (and is independent from $x_{R,s}$).

The term $\kappa_s x_{R,s}$ in equation (1) represents the mobilization of reserve biomass (when viewed from inside the microbial cell). Note that the original DEB interpretation of $\kappa_s x_{R,s}$ does not emphasize this view from inside the microbial cell. However, by following the observation that intracellular enzymatic reactions can often be modeled with the law of mass action using intracellular substrate and enzyme concentrations as primary variables (e.g., Ciliberto et al., 2007; Tadmor and Tlusty, 2008; Vasilescu et al., 2013; Etienne et al., 2020), such a viewpoint enables us to revise the sDEB model with the ECA kinetics introduced later (section 2.2). Reserve mobilization described by $\kappa_s x_{R,s}$ is apparently based on first order chemistry kinetics, with $x_{R,s}$ representing the concentration of reserve biomass inside the container formed by structural biomass (which defines the volumetric space where reserve biomass is biochemically modified). Corresponding to this representation, the reserve density dynamics are independent of biological growth or mortality. However, when the reserve biomass dynamics are described in the non-normalized form (i.e., when reserve dynamics are viewed from outside the microbial cell, which for a population include contributions from all living cells and $x_{R,s}$ is the mean reserve biomass density), the effect of growth and mortality emerges:

$$\frac{dX_{R,s}}{dt} = \frac{d\left(X_{V,s}x_{R,s}\right)}{dt} = X_{V,s}\frac{dx_{R,s}}{dt} + \frac{dX_{V,s}}{dt}x_{R,s} = J_{A,s} - J_{RV,s} - \gamma_{M,s}X_{R,s}, \tag{2}$$

where $J_{A,s} = j_{A,s}X_{V,s}$ (gC m^{-3} s^{-1}), $\gamma_{M,s}$ (s^{-1}) is specific biomass loss rate by mortality, and $J_{RV,s}$ is the gross flux of reserve mobilization:

$$J_{RV,s} = \left(\kappa_s - g_{V,s}\right)X_{R,s}, \tag{3}$$

while the specific changing rate of structural biomass is

$$\frac{1}{X_{V,s}}\frac{dX_{V,s}}{dt} = g_{V,s} - \gamma_{M,s}, \tag{4}$$

where $g_{V,s}$ (s^{-1}) is positive growth obtained by equating $J_{RV,s}$ in equation (3) with its aimed use i.e., $(m_{V,s}/Y_{RV,s} + g_{V,s}/Y_{RV,s})X_{V,s}$ (also see Fig. 1a):

$$g_{V,s} = \frac{\kappa_s x_{R,s} - m_{V,s}/Y_{RV,s}}{x_{R,s} + 1/Y_{RV,s}}, \tag{5}$$

where $m_{V,s}$ (s^{-1}) is specific maintenance respiration for the structural biomass and $Y_{RV,s}$ is the conversion efficiency from the reserve biomass into structural biomass. When $\kappa_s x_{R,s} < m_{V,s}/Y_{RV,s}$, it leads to $g_{V,s} < 0$, implying reserve mobilization deficit for maintenance respiration. To make up this deficit, senescence of structural biomass occurs (i.e., $dX_{V,s}/dt < 0$ so that the nominal value of $g_{V,s}$ from equation (5) is negative), resulting in population loss. For convenience of computation, we lumped this population loss into to the mortality term $\gamma_{M,s}$ (although a more complicated scheme is possible by allowing concurrent degradation of structural biomass to support maintenance (Tolla et al., 2007)).

While the sDEB model has been quite successful in numerous applications (Kooijman, 2009), two assumptions underlying its formulation can be improved. First, since the reserve dynamics shown in equation (1) are derived from Euler's theorem for homogeneous functions (Apostol, 1967) to satisfy the partition principle, the sDEB model effectively assumes that (when viewed from intracellular space) reserve mobilization (as represented by reserve density dynamics in equation (1)) is effectively a one-step linear process, although many steps of enzyme catalysis are usually involved and the gross reserve mobilization flux $J_{RV,s}$ is still a nonlinear function of reserve density due to the growth-induced dilution effect as shown in equations (3) and (5). However, as reserve biomass is mobilized through enzymatic processes (Madigan et al., 2009), at least two steps are involved: (1) enzymes bind to substrate molecules to form enzyme-substrate complexes, and (2) the enzyme-substrate complexes release product molecules. Therefore, reserve biomass mobilization dynamics should be nonlinear when viewed from inside the cell, as is often formulated in the literature by the law of mass action with intracellular enzyme and metabolite concentrations as primary variables (Ciliberto et al., 2007; Tadmor and Tlusty, 2008), where the reaction volume is delineated by structural biomass. Since intracellular enzymes and metabolites are major constituents of reserve biomass in the DEB framework (Kooijman, 2009), the upscaled reserve dynamics should be non-linear and have reserve density as one of its primary variables. Further, with the goal of developing logically consistent mathematical theories (such as the generalization of positive integers into rational numbers where operations of addition and multiplication are maintained), the sDEB model should be coherent with the more detailed mechanistic flux balance approaches that directly integrate kinetics in gene and protein networks, as have been widely used in molecular studies of bacteria and fungi (e.g., Chowdhury et al., 2014; Labhsetwar et al., 2014; Labhsetwar et al., 2017). This coherency (i.e., maintaining the mathematic structure of the kinetics when compared to more detailed models such as the flux balance models) is apparently not achieved with the linear dynamics of reserve density in the sDEB model, although the sDEB model is scaling consistent with flux balance analysis when metabolic fluxes are used as primary variables (which then leads to a linear system). Second, the sDEB model assumes that only reserve biomass can fuel metabolic activities of an organism, but Tolla et al. (2007) suggested that structural biomass has to be degraded to fuel maintenance respiration that cannot be fully supported by mobilized reserves, e.g., in the case of starvation. While the second shortcoming is conceptually less serious than the first, it incurs numerical iterations in the calculation of structural biomass growth (because the growth rate becomes a nonlinear function of itself; see equation C.2 in Tolla et al. (2007)), which could be cumbersome when the sDEB model is used to construct agent-based models, where hundreds or thousands of organisms are represented (e.g., Wilmoth et al., 2018). Addressing these two shortcomings could benefit the development of a unified model of biological growth.

2.2. Enzyme-regulated reaction network representation

To develop a more explicit and scaling consistent representation of reserve dynamics in the rDEB model, we need a formulation to quantify interactions between multiple enzymes and substrates. In our previous study of enzyme-regulated reaction networks that involve many enzymes and many substrates, we derived the ECA kinetics based on law of mass action, and found the ECA kinetics having scaling properties that allow one to merge or partition substrates and enzymes (Tang and Riley, 2013, 2017), particularly when many substrates are consumed by a single enzyme. Specifically, when N types of substrates S_j $(j = 1, \cdots, N)$ are being consumed by enzyme E, the consumption rate F_j of S_j by enzyme E can be approximated using ECA kinetics as

$$F_j = \frac{v_{max,j} S_{j,T} E_T / K_j}{1 + \sum_i S_{i,T}/K_i + E_T/K_j}; \quad (6)$$

and the total substrate consumption by E is

$$F = \sum_j F_j = E_T \sum_j \frac{v_{max,j} S_{j,T}/K_j}{1 + \sum_i S_{i,T}/K_i + E_T/K_j}, \quad (7)$$

where $v_{max,j}$ is the maximum consumption rate of S_j, K_j is the dissociation parameter for enzyme E with respect to substrate S_j, and subscript T designates total concentration of a given variable (defined with respect to the intracellular space when applied to the reserve dynamics of the rDEB model).

We show below that ECA kinetics also satisfies the partition principle as required by the DEB theory for reserve dynamics. Specifically, if all these substrates are metabolically equivalent, that is, they have the same Gibbs free energy density or are just the same substrate numerically tagged differently (e.g., by the elapsed time when these molecules are added to the reaction system), we have $K_j = K_S$, and $v_{max,j} = v_{max}$, such that equation (6) becomes

$$F_j = \frac{v_{max} E_T/K_S}{1 + \left(\sum_i S_{i,T}\right)\Big/ K_S + E_T/K_S} S_{j,T} = \frac{v_{max} E_T/K_S}{1 + S_T/K_S + E_T/K_S} S_{j,T}, \quad (8)$$

where $S_T = \sum_i S_{i,T}$.

Accordingly, equation (7) becomes

$$F = \frac{v_{max} E_T/K_S}{1 + S_T/K_S + E_T/K_S} \sum_j S_{j,T} = \frac{v_{max} E_T/K_S}{1 + S_T/K_S + E_T/K_S} S_T. \quad (9)$$

In particular, from equations (8) and (9), we have the partition relationship

$$\frac{F_j}{F} = \frac{S_{j,T}}{S_T}, \quad (10)$$

which states that component flux F_j is proportional to the component substrate concentration $S_{j,T}$, thus justifying our use of ECA kinetics to derive the rDEB model in section 2.3, below.

ECA kinetics have recently been successfully used to model enzyme and mRNA interactions in bacterial cells (Etienne et al., 2020), plant-soil competition of nutrients in land ecosystems (Zhu et al., 2016, 2019a), and microbial competition for substrates in aqueous environments (Cheng et al., 2019; Barnum et al., 2020) and during litter decomposition (Wang and Allison, 2019). Therefore, applying ECA kinetics to improve the reserve dynamics of the DEB model may help bridge the gap between intracellular flux-balance analysis or metabolic models for individuals, and DEB models for individuals and populations. Such a bridging could facilitate upscaling of these more complex models and thereby enable a unified mathematical treatment in the field of microbial biogeochemistry modeling.

We next present the three-compartment revised DEB (rDEB) model.

2.3. The revised DEB model

To address the two limitations of the sDEB model described above (i.e., the assumption of linear reserve density dynamics and the numerical difficulty induced by using structural biomass to make up the reserve mobilization deficit for maintenance during starvation) and to bridge the DEB theory with metabolic modeling, we derive the rDEB model below. We achieved this revision by classifying microbial biomass into reserve, kinetic, and structural compartments (Fig. 1b), and representing reserve density dynamics using ECA kinetics.

2.3.1. Dynamics of the reserve biomass compartment

When viewed from inside the microbial cell, reserve biomass is mobilized by enzymes (termed as kinetic biomass $X_{N,r}$ in the rDEB model) with the intracellular space (defined as the space circumscribed by plasma membranes) as the reaction volume,

$$\frac{dx_{R,r}}{dt} = j_{A,r} - j_{RN,r} + \frac{x_{N,r}}{\tau_{N,r}}, \quad (11)$$

where $x_{R,r} = X_{R,r}/X_{V,r}$ is reserve biomass density, $x_{N,r} = X_{N,r}/X_{V,r}$ is kinetic biomass density, $j_{A,r} = J_{A,r}/X_{V,r}$ is the normalized substrate assimilation rate, $\tau_{N,r}$ is the turnover time of kinetic biomass (including enzymes), and $j_{RN,r}$ is intracellular enzyme-catalyzed reserve mobilization. (Kinetic biomass turnover is caused by lysis enzymes, which are part of the kinetic biomass, and could be explicitly represented by further disaggregating kinetic biomass into more compartments. Also, lysed kinetic biomass becomes reserve biomass, closing the coupling with reserve biomass.)

With the delineation of reserve and kinetic biomass compartments, $j_{RN,r}$ can be approximated with ECA kinetics:

$$j_{RN,r} = \frac{\alpha_r \kappa_{max,r} x_{N,r}}{K_{R,r} + x_{R,r} + \alpha_r x_{N,r}} x_{R,r} = \kappa_r x_{R,r}, \quad (12)$$

where α_r is the number of binding sites for reserve biomass per unit of kinetic biomass, and κ_r, the rDEB analog to parameter κ_s in the sDEB model, is

$$\kappa_r = \frac{\alpha_r \kappa_{max,r} x_{N,r}}{K_{R,r} + x_{R,r} + \alpha_r x_{N,r}}. \quad (13)$$

Calculation of the affinity parameter $K_{R,r}$ (as a function of intracellular content) between kinetic biomass and reserve biomass is described in section 2.3.3 (and section A of the supplemental material).

For structural biomass, we have

$$\frac{1}{X_{V,r}} \frac{dX_{V,r}}{dt} = g_{V,r} - \gamma_{M,r}, \quad (14)$$

where $g_{V,r}$ is the positive specific growth rate (and, similar to the sDEB model, negative $g_{V,r}$, when it occurs, is grouped into $\gamma_{M,r}$), and $\gamma_{M,r}$ is the specific mortality rate.

Analogous to equation (2), for the non-normalized form of reserve biomass, we have

$$\frac{dX_{R,r}}{dt} = J_{A,r} - J_{RN,r} - \gamma_{M,r} X_{R,r} + \frac{X_{N,r}}{\tau_{N,r}}. \quad (15)$$

Meanwhile, from the product rule of derivatives, we have

$$\frac{dX_{R,r}}{dt} = \frac{d}{dt}\left(x_{R,r} X_{V,r}\right) = X_{V,r} \frac{dx_{R,r}}{dt} + x_{R,r} \frac{dX_{V,r}}{dt}. \quad (16)$$

Thence by aid of equations (11) and (12) and (14)–(16), we obtain the gross reserve mobilization flux $J_{RN,r}$, the counterpart of $J_{RV,s}$ in equation (3):

$$J_{RN,r} = X_{V,r} j_{RN,r} - g_{V,r} X_{R,r} = j_{RN,r} X_{V,r} = \left(\kappa_r - g_{V,r}\right) X_{R,r}. \quad (17)$$

Because κ_r is a function of $x_{R,r}$, reserve biomass density decays as a nonlinear function of reserve density ($x_{R,r}$; equation (12)). However, when $K_{R,r} + \alpha_r x_{N,r} \gg x_{R,r}$, i.e., reserve density is sufficiently low, $\kappa_r \approx \alpha_r \kappa_{max,r} x_{N,r} / (K_{R,r} + \alpha_r x_{N,r})$, which is a function of only the kinetic biomass density $x_{N,r}$. In this case, reserve biomass mobilization $J_{RN,r}$ becomes a pseudo linear function of reserve biomass (because $g_{V,r}$ is a nonlinear function of reserve biomass density):

$$J_{RN,r} = \left(\frac{\alpha_r \kappa_{max,r} x_{N,r}}{K_{R,r} + \alpha_r x_{N,r}} - g_{V,r}\right) X_{R,r}, \quad (18)$$

similar to how $J_{RV,s}$ is formulated in equation (3) for the sDEB model.

To make an analog to the sDEB model, by considering kinetic

biomass $X_{N,r}$ and structural biomass $X_{V,r}$ (in the rDEB model) together to be the sDEB "structural biomass ($X_{V,s}$)" and treat $x_{N,r}$ as a constant, we have

$$\kappa_s = \kappa_r = \frac{\alpha_r \kappa_{max,r} x_{N,r}}{K_{R,r} + \alpha_r x_{N,r}}. \tag{19}$$

From equation (19), we see that the specific reserve turnover rate κ_s in the sDEB model (equation (1)) is a function of intracellular enzyme abundance (as represented by $x_{N,r}$), and the linear reserve density dynamics is a good approximation only when reserve density $x_{R,r}$ is low (compared to $K_{R,r} + \alpha_r x_{N,r}$). Moreover, since kinetic biomass is primarily comprised of proteins, equation (19) suggests that the sDEB model implicitly assumes constant proteomic distributions (i.e., the relative distribution of types of proteins and thus kinetic traits inside the cell does not vary). Compared to the linear decay rule of reserve density in the sDEB model, the nonlinear decay rule of reserve density (i.e., equation (12)) in the rDEB model can account for the macromolecular crowding effect (Minton, 1998; Chebotareva et al., 2004) on potential growth rate reduction at high reserve density or under osmotic stress, where the latter contributes to a mechanistic explanation of how moisture stress affects microbial activity. From equation (12) for $j_{RN,r}$, the mobilization rate of reserve biomass density, we see that, during the growth of a microbial cell, the macromolecular crowding effect can modify $\kappa_{max,r}$ and $K_{R,r}$, and consequently κ_r, the specific decay rate of reserve biomass density. We will further discuss the macromolecular crowding effect in section 2.3.3.

2.3.2. Dynamics of the kinetic and structural biomass compartments

In the 3-compartment rDEB model, growth of kinetic biomass and structural biomass are driven by the mobilized reserve flux. Specifically, the dynamics of kinetic biomass density is

$$\frac{dx_{N,r}}{dt} = \frac{d}{dt}\left(\frac{X_{N,r}}{X_{V,r}}\right) = Y_{RN,r} f_{N,r} j_{RN,r} - \frac{x_{N,r}}{\tau_{N,r}} = Y_{RN,r} f_{N,r} \kappa_r x_{R,r} - \frac{x_{N,r}}{\tau_{N,r}}. \tag{20}$$

where parameter $f_{N,r}$ designates the portion of mobilized reserve flux used to produce new kinetic biomass (thus to some extent $f_{N,r}$ is equivalent to the ribosome effort allocated to kinetic biomass growth). When equation (20) is written in the non-normalized form (while taking reference of Fig. 1b),

$$\begin{aligned} \frac{dX_{N,r}}{dt} &= Y_{RN,r} J_{RN,r,1} - \frac{X_{N,r}}{\tau_{N,r}} - \gamma_{M,r} X_{N,r} = X_{V,r}\frac{dx_{N,r}}{dt} + \frac{X_{N,r}}{X_{V,r}}\frac{dX_{V,r}}{dt} \\ &= Y_{RN,r} f_{N,r} \kappa_r X_{R,r} - \frac{X_{N,r}}{\tau_{N,r}} + (g_{V,r} - \gamma_{M,r}) X_{N,r}, \end{aligned} \tag{21}$$

from which the mobilized reserve flux from $X_{R,r}$ to $X_{N,r}$ is derived as

$$J_{RN,r,1} = f_{N,r} \kappa_r X_{R,r} + g_{V,r} X_{N,r} / Y_{RN,r}. \tag{22}$$

Combining equation (22) with the flux balance relationship between $J_{RN,r}$, $J_{RN,1}$, and $J_{RN,2}$ shown in Fig. 1b, the mobilized reserve going to structural biomass has the following relationship with the structural biomass maintenance ($m_{V,r}$) and growth ($g_{V,r}$, assuming $g_{V,r} > 0$) as

$$J_{RN,r,2} = J_{RN,r} - J_{RN,r,1} = (1 - f_{N,r}) \kappa_r X_{R,r} - g_{V,r}(X_{R,r} + X_{N,r} / Y_{RN,r}) = X_{V,r}(m_{V,r} + g_{V,r}) / Y_{RV,r}. \tag{23}$$

From equation (23), we obtain:

$$g_{V,r} = \frac{(1 - f_{N,r}) \kappa_r x_{R,r} - m_{V,r} / Y_{RV,r}}{\frac{1}{Y_{RV,r}} + \frac{x_{N,r}}{Y_{RN,r}} + x_{R,r}}. \tag{24}$$

Table 1
Governing equations of the revised dynamic energy budget model (rDEB) and the standard dynamic energy budget model (sDEB).

rDEB model	sDEB model
Reserve biomass dynamics: $\frac{dX_{R,r}}{dt} = J_{A,r} - (\kappa_r - g_{V,r}) X_{R,r} - \gamma_{M,r} X_{R,r} + \frac{X_{N,r}}{\tau_{N,r}}$.	Reserve biomass dynamics: $\frac{dX_{R,s}}{dt} = J_{A,s} - (\kappa_s - g_{V,s}) X_{R,s} - \gamma_{M,s} X_{R,s}$.
Kinetic biomass dynamics: $\frac{dX_{N,r}}{dt} = Y_{RN,r} f_{N,r} \kappa_r X_{R,r} + (g_{V,r} - \gamma_{M,r}) X_{N,r} - \frac{X_{N,r}}{\tau_{N,r}}$.	
Structural biomass dynamics: $\frac{dX_{V,r}}{dt} = (g_{V,r} - \gamma_{M,r}) X_{V,r}$.	Structural biomass dynamics: $\frac{dX_{V,s}}{dt} = (g_{V,s} - \gamma_{M,s}) X_{V,s}$.
Specific reserve mobilization rate: $\kappa_r = \frac{\alpha_r \kappa_{max,r} x_{N,r}}{K_{R,r} + x_{R,r} + \alpha_r x_{N,r}}$.	Specific reserve mobilization rate: κ_s.
Population growth rate: $g_{V,r} = \frac{(1 - f_{N,r}) \kappa_r x_{R,r} - m_{V,r} / Y_{RV,r}}{\frac{1}{Y_{RV,r}} + \frac{x_{N,r}}{Y_{RN,r}} + x_{R,r}}$.	Population growth rate: $g_{V,s} = \frac{\kappa_s x_{R,s} - m_{V,s} / Y_{RV,s}}{\frac{1}{Y_{RV,s}} + x_{R,s}}$.

Equation (24) together with $\gamma_{M,r}$ defines the dynamics of structural biomass as

$$\frac{dX_{V,r}}{dt} = (g_{V,r} - \gamma_{M,r}) X_{V,r}, \tag{25}$$

We thus have the rDEB model formulated by equations (((13), (15), (17), (21), (24) and (25), as summarized in Table 1.

2.3.3. Parameterization of κ_r, the specific decay rate of reserve biomass density

κ_r is influenced by two types of macromolecular crowding effects: (1) the chemical activity of reactants and products (Minton, 1990), and (2) the collision rate (characterized by diffusion) among these different chemical species (Dix and Verkman, 2008). Chemical activities increase with increasing crowding agents (i.e., macromolecules that have mass from 50 to 200 kD), therefore crowding effects can increase chemical reaction rates. Further, since intracellular enzymatic reactions are often diffusion limited, the affinity parameter $K_{R,r}$ (used in equation (13) for the definition of κ_r) is (approximately) proportional to $1/D_E$, where D_E is effective enzyme diffusivity with respect to the substrates in the cytosol. Because D_E decreases with increasing crowding agents (due to increased tortuosity), $K_{R,r}$ increases and thus κ_r decreases. As a first approximation for D_E, we take an analogy to the tortuosity effect on diffusion in soil:

$$D_E = D_{E0}\left(1 - \varphi_V\left(1 + x_{N,r} d_N + x_{R,r} d_R\right)\right)^{\sigma}\left(1 + \frac{\Pi - \Pi_0}{\varepsilon}\right)^{\sigma}, \tag{26}$$

where D_{E0} is the reference diffusivity, σ is set to 2 by assuming the intracellular tortuosity resembles that in a soil (Moldrup et al., 2003; Vasilescu et al., 2013); terms in $(1 - \varphi_V(1 + x_{N,r} d_N + x_{R,r} d_R))^{\sigma}$ represent the crowding effect, with φ_V being the cellular space taken up by the structural biomass and is a linear function of genome size (which is inferred to decrease with cell size for bacteria (Kempes et al., 2016)), d_N is the ratio of mass density of structural biomass to non-structural biomass (estimated as 1.1 using data synthesized in Milo and Phillips (2015)), and d_R is the ratio of mass density of structural biomass to reserve biomass (estimated as 0.8 using data synthesized in Milo and

Phillips (2015)). Details of the estimation of d_N and d_R are given in section A of the supplemental material. Terms in $\left(1+\frac{\Pi-\Pi_0}{\varepsilon}\right)^{\sigma}$ represent the effect of turgor pressure Π on cell volume (using results from Steudle et al., 1977), which changes as a function of osmotic pressure and external pressure (ε is elasticity of the cell). For soil microbes, it can be inferred that as soil moisture decreases, D_E decreases, then turgor pressure decreases from full turgor Π_0, and $K_{R,r}$ will increase to slow down microbial metabolism, triggering either dormancy or death. We leave discussion on this topic to future work.

Using the approach from Tang and Riley (2019) (i.e., the relationship $K_{R,r} \propto 1/D_E$), together with equation (26), we can approximate $K_{R,r}$ as

$$K_{R,r} = K_{R0}\left(1-\varphi_V\left(1+x_{N,r}d_N+x_{R,r}d_R\right)\right)^{-2}\left(1+\frac{\Pi-\Pi_0}{\varepsilon}\right)^{-\sigma}, \quad (27)$$

where $K_{R0} = \kappa_{max}\omega_V M_w/(4\pi r_E D_{E0} N_A)$, with r_E being the radius of enzyme molecules, which is typically a few nanometers (Milo and Phillips, 2015). The typical value of D_{E0} is about 1 $\mu m^2\ s^{-1}$, N_A is the Avogadro number (molecules $mole^{-1}$), and ω_V (m^3 per unit structural biomass) is a parameter that converts structural biomass into total intracellular space by $\omega_V X_V$ and M_w (so that K_{R0} is unitless, like reserve and kinetic biomass density; see section A of the supplemental material for more details).

In section A of the supplemental material, we developed an estimate of K_{R0} for bacteria (as a representative of prokaryotes) and typical eukaryotes, and found that K_{R0} is usually much smaller than $x_{R,r} + \alpha_r x_{N,r}$, and therefore the macromolecular crowding effect (manifested as diffusion limitation) on $K_{R,r}$ is significant only when the cell is under severe volume reduction or turgor loss (i.e., the last term in equation (27) is large). This inference is consistent with the finding by Tadmor and Tlusty (2008), who showed for *E. coli* that the macromolecular crowding effect on diffusion is not significant under normal conditions. This comparison also implies that moisture stress affects microbial activity primarily through its control of substrate diffusion to the microbes in the soil, which for the rDEB model is through its influence on $J_{A,r}$ (and analogously for the sDEB model through its influence on $J_{A,s}$).

2.3.4. Parameterization of $f_{N,r}$

In the rDEB model, $f_{N,r}$ represents the fraction of metabolic effort used to construct kinetic biomass, which is made up of RNAs and proteins. Therefore, $f_{N,r}$ is a dynamic function of proteomics (i.e., the relative distribution of intracellular proteins). Proteins in the kinetic biomass compartment are separated into ribosome proteins and others that provide metabolic flux to synthesize structural biomass, kinetic biomass, extracellular enzymes, and excretions. However, achieving this detail requires us to track the RNA pools explicitly, and introduce at least four more parameters related to protein elongation rate, fraction of protein in structural biomass, the RNA to protein ratio associated with ribosome, and RNA to protein ratio during translation. We thus prescribe $f_{N,r}$ with a static value and show in section 4.2 that this choice reveals a potentially important over-simplification in the sDEB model.

2.3.5. Parameterization of specific maintenance respiration rate $m_{V,r}$

Based on the Pirt model of microbial growth, Kempes et al. (2017) included the costs of protein repair, RNA repair, motility, and proton gradients in their calculation of maintenance respiration. In the rDEB model, the structural biomass compartment only includes DNA and its associated proteins and cell wall membrane materials that support the minimal survival of a bacterial cell (which require some amount of ribosome and metabolic proteins in the kinetic biomass compartment, and thereby a minimal proton motive force). Therefore, the rDEB maintenance respiration only accounts for a fraction of the costs defined in Kempes et al. (2017). Accordingly, the extra costs associated with structural biomass repair during active growth is regarded as part of growth respiration.

With our definition, under zero growth rate, i.e., $g_{V,r} = 0$, from equation (24) we have

$$m_{V,r} = Y_{RV,r}\left(1-f_{N,r}\right)\kappa_r x_{R,r} = Y_{RV,r}\left(1-f_{N,r}\right)\frac{\alpha_r \kappa_{max,r} x_{N,r} x_{R,r}}{K_{R,r}+x_{R,r}+\alpha_r x_{N,r}}. \quad (28)$$

Equation (28) suggests that even when all reserve flux to structural biomass is used for maintenance respiration (i.e., $f_{N,r}$ is very close to zero), kinetic biomass may still increase, which will lead to higher $x_{N,r}$ to temporarily make up for the maintenance respiration deficit. However, higher $x_{N,r}$ will lead to greater turnover of $x_{N,r}$, and when the reserve biomass increments of $x_{R,r}$ from the assimilation of external substrates fail to match this faster turnover, kinetic biomass will be re-translocated into reserve biomass to temporarily support the survival of the microbe. This result indicates that $f_{N,r}$ should be dynamic, as reserve biomass is more likely to be used first to fulfill maintenance costs when the mobilized reserve flux is small.

2.3.6. Total respiration associated with reserve biomass mobilization

Corresponding to the three biomass compartments in the rDEB model (Fig. 1b), the total respiration associated with the reserve biomass mobilization ($R_{M,r}$) includes contributions from the construction of kinetic biomass and structural biomass (i.e., growth respiration), and the cost for maintaining cellular integrity (maintenance respiration):

$$R_{M,r} = \left(1-Y_{NR,r}\right)\left(f_{N,r}\kappa_r X_{R,r}+\frac{g_{V,r}}{Y_{NR,r}}X_{N,r}\right)+\left[\frac{m_{V,r}}{Y_{RV,r}}+g_{V,r}\left(\frac{1}{Y_{RV,r}}-1\right)\right]X_{V,r}, \quad (29)$$

when $g_{V,r} \geq 0$, and

$$R_{M,r} = \left(1-Y_{NR,r}\right)f_{N,r}\kappa_r X_{R,r}+\left(1-f_{N,r}\right)\kappa_r X_{R,r}, \quad (30)$$

when $g_{V,r} < 0$.

For the sDEB model, the corresponding equations are

$$R_{M,s} = \left[\frac{m_{V,s}}{Y_{RV,s}}+g_{V,s}\left(\frac{1}{Y_{RV,s}}-1\right)\right]X_{V,s}, \quad (31)$$

when $g_{V,s} \geq 0$, and

$$R_{M,s} = \kappa_s X_{R,s}, \quad (32)$$

when $g_{V,s} < 0$.

When the respiration from substrate assimilation (i.e., that associated with $J_{A,r}$ or $J_{A,s}$) is added to $R_{M,r}$ (or $R_{M,s}$), we obtain the total respiration $R_{T,r}$ in the rDEB model or $R_{T,s}$ in the sDEB model.

3. Example applications

In the following, we compare the rDEB and sDEB models with some empirical models (i.e., the compromise model for microbial growth (Wang and Post, 2012), the quadratic model for tradeoff between specific bulk repatriation and specific growth rate (Vikstrom and Wikner, 2019), and the power law model for tradeoff between substrate uptake rate and biomass yield (Calabrese et al., 2021)) using three examples. We note that all variables related to the compromise model are subscripted with "c".

3.1. Comparison for an exponentially growing bacterial population

We first compare some theoretical results (i.e., specific growth rate μ, specific substrate uptake rate q, and specific total respiration rate R_b) from the compromise model (Beeftink et al., 1990; Wang and Post, 2012), rDEB model, and sDEB model for an exponentially growing population feeding on a limiting substrate S (e.g., glucose). Under this condition, the rDEB model implies constant biomass composition, i.e., $dx_{R,r}/dt = 0$ and $dx_{N,r}/dt = 0$ (which ensure $dX_{R,r}/dt = g_{v,r}X_{R,r}$ and $dX_{N,r}/dt = g_{v,r}X_{N,r}$). Likewise, $dx_{R,s}/dt = 0$ holds for the sDEB model. Further, to simplify the comparison, all models assume zero mortality or

include mortality in the maintenance respiration. Therefore, the DEB models derived in this section are not for generic conditions where different biomass compartments may evolve asynchronously. Additionally, taking carbon as the chemical element of interest, for all three models, there exists the relationship that carbon uptake rate equals the sum of net increasing rate of living microbial biomass carbon and total carbon respiration rate. This relationship does not hold for more generic conditions where mortality, extracellular enzyme production and changes in microbial elemental stoichiometry are significant (Tang and Riley, 2015).

Based on Wang and Post (2012), we have for the compromise model:

$$\mu_c(S) = \mu_{max,c} h(S) - m_{q,c}[1 - h(S)], \tag{33}$$

$$q_c(S) = \mu_c(S)/Y_{G,c} + m_{q,c}/Y_{G,c} = \mu_{max,c} h(S)/Y_{G,c} + m_{q,c} h(S)/Y_{G,c}, \tag{34}$$

$$R_{b,c}(S) = \left(\frac{1}{Y_{G,c}} - 1\right)\mu_c(S) + \frac{m_{q,c}}{Y_{G,c}}, \tag{35}$$

where $\mu_c(S)$ is the specific net growth rate whose maximum value is $\mu_{max,c}$; $q_c(S)$ is the specific substrate uptake rate, with a substrate use efficiency $Y_{G,c}$ (also called as "true" growth yield; Wang and Post, 2012); $m_{q,c}$ is the physiological maintenance factor (which was used to define the total maintenance respiration m_T in equation (20) of (Wang and Post, 2012)); $h(S)$ is the dimensionless functional response to substrate availability (e.g., $h(S) = S/(K_S + S)$ when adopting the Michaelis-Menten kinetics); and $R_{b,c}$ is the specific bulk respiration computed by subtracting $\mu_c(S)$ from $q_c(S)$ using the mass conservation relationship for an exponentially growing population that substrate uptake $q_c(S)$ equals to the sum of net increase of biomass $\mu_c(S)$ and total respiration $R_{b,c}(S)$ (but this relationship does not hold under more general conditions, where mortality, exudation are significant, as we explained at the beginning of this section). The compromise model improves upon the Pirt model (Pirt, 1965) and Herbert model (e.g., Dawes and Ribbons, 1962) by incorporating the empirical observation that biomass yield increases with specific growth rate (thus it is an empirical model).

For the rDEB model (derived in section B in the supplemental material), we have specific net growth rate

$$\mu_r(S) = (1 - f_{N,r})\kappa_r \frac{x_{R,r}}{\frac{1}{Y_{RV,r}} + \frac{x_{N,r}}{Y_{RN,r}} + x_{R,r}} - \frac{m_{V,r}/Y_{RV,r}}{\frac{1}{Y_{RV,r}} + \frac{x_{N,r}}{Y_{RN,r}}}\left(1 - \frac{x_{R,r}}{\frac{1}{Y_{RV,r}} + \frac{x_{N,r}}{Y_{RN,r}} + x_{R,r}}\right), \tag{36}$$

and specific substrate uptake rate

$$q_r(S) = \frac{j_{A,r}}{Y_{SR,r}} = \frac{\mu_r(S)}{Y_{SR,r}Y_{RV,r}} \frac{(1 - Y_{RN,r}f_{N,r})\kappa_r}{(1 - f_{N,r})\kappa_r - (1 + \tau_{N,r}f_{N,r}\kappa_r)\mu_r(S)} + \frac{m_{V,r}}{Y_{SR,r}Y_{RV,r}} \frac{(1 - Y_{RN,r}f_{N,r})\kappa_r}{(1 - f_{N,r})\kappa_r - (1 + \tau_{N,r}f_{N,r}\kappa_r)\mu_r(S)}. \tag{37}$$

From equation (36), we find that the specific growth rate $\mu_r(S)$ in the rDEB model has a similar form as $\mu_c(S)$ in equation (33) for the compromise model, except that in the rDEB model, $\mu_r(S)$ is a function of reserve biomass density $x_{R,r}$ or cellular nutrient quota as used in the empirically formulated Droop model (Droop, 1974). Further, the specific substrate uptake rate $q_r(S)$ is nonlinearly related to the specific growth rate $\mu_r(S)$ for the rDEB model (equation (37)) rather than linearly for the compromise model (equation (34)).

By relating $x_{R,r}$ and $x_{N,r}$ with external substrate concentration (as enabled by the assumed exponential growth) using an assimilation flux parameterized by $q_r(S) \bullet Y_{SR,r} = j_{A,r} = a_{max,r}S/(K_{S,r} + S)$, equations (36) and (37) for the rDEB model can be written as

$$\mu_r(S) = \mu_{max,r}\overline{h}_r(S) - m_{q,r}[1 - \overline{h}_r(S)], \tag{38}$$

$$q_r(S) = \frac{\mu_r(S)}{Y_{G,r}} + \frac{m_{q,r}}{Y_{G,r}} = \frac{\mu_{max,r}}{Y_{G,r}}\overline{h}_r(S) + \frac{m_{q,r}}{Y_{G,r}}\overline{h}_r(S), \tag{39}$$

and the corresponding specific bulk respiration is found as

$$R_{b,r}(S) = \left(\frac{1}{Y_{G,r}} - 1\right)\mu_r(S) + \frac{m_{q,r}}{Y_{G,r}}, \tag{40}$$

where

$$\mu_{max,r} = \frac{Aa_{max,r}}{c_1 + c_2 a_{max,r}}\left(1 - \frac{m_{V,r}}{AY_{RV,r}a_{max,r}}\right), \tag{41}$$

$$\overline{h}_r(S) = \frac{S}{\frac{c_1 K_{S,r}}{c_1 + c_2 a_{max,r}} + S} = \frac{S}{\overline{K}_{S,r} + S}, \tag{42}$$

$$m_{q,r} = \frac{m_{V,r}}{Y_{RV,r}c_1}, \tag{43}$$

$$c_1 = \frac{1}{Y_{RV,r}} + \frac{K_{R,r}}{\alpha_r \kappa_{max,r}\tau_{N,r}Y_{RN,r}f_{N,r} - 1}, \tag{44}$$

$$c_2 = \left(\frac{1}{Y_{RN,r}} + \frac{\alpha_r}{\alpha_r\kappa_{max,r}\tau_{N,r}Y_{RN,r}f_{N,r} - 1}\right)\frac{\tau_{N,r}Y_{RN,r}f_{N,r}}{1 - Y_{RN,r}f_{N,r}}, \tag{45}$$

$$A = \frac{1 - f_{N,r}}{1 - Y_{RN,r}f_{N,r}}, \tag{46}$$

and

$$Y_{G,r} = \frac{Y_{SR,r}}{c_1}(A - c_2\mu_r(S)). \tag{47}$$

Therefore, both $\mu_r(S)$ and $q_r(S)$ for the rDEB model have the same form as $\mu_c(S)$ and $q_c(S)$ for the compromise model. Thus, our derivation lends some mechanistic support to the empirical equation for $\mu_c(S)$ in the compromise model, and reveals that the compromise model fails to represent the "true" growth yield $Y_{G,r}$ as a decreasing function of growth rate (see equation (47)). Accordingly, the specific bulk respiration $R_{b,r}$ is also a nonlinear function of growth rate, rather than a linear function as formulated in equation (35) for the compromise model.

Similarly, for the sDEB formulation (see section C in the supplemental material), we have specific net growth rate $\mu_s(S)$, specific substrate uptake rate $q_s(S)$ and specific bulk respiration $R_{b,s}(S)$ as

$$\mu_s(S) = \mu_{max,s}\overline{h}_s(S) - m_{V,s}[1 - \overline{h}_s(S)], \tag{48}$$

$$q_s(S) = \frac{\mu_s(S)}{Y_{G,s}} + \frac{m_{V,s}}{Y_{G,s}} = \frac{\mu_{max,s}}{Y_{G,s}}\overline{h}_s(S) + \frac{m_{V,s}}{Y_{G,s}}\overline{h}_s(S), \tag{49}$$

$$R_{b,s}(S) = \left(\frac{1}{Y_{G,s}} - 1\right)\mu_s(S) + \frac{m_{V,s}}{Y_{G,s}}, \tag{50}$$

where

$$\overline{h}_s(S) = \frac{S}{\frac{\kappa_s K_{S,s}}{\kappa_s + a_{max,s}Y_{RV,s}} + S} = \frac{S}{\overline{K}_{S,s} + S}, \tag{51}$$

$$\mu_{max,s} = \frac{\kappa_s Y_{RV,s}a_{max,s}}{\kappa_s + Y_{RV,s}a_{max,s}}\left(1 - \frac{m_{V,s}}{Y_{RV,s}a_{max,s}}\right), \tag{52}$$

$$Y_{G,s} = Y_{SR,s}Y_{RV,s}(1 - \mu_s(S)/\kappa_s). \tag{53}$$

Once again, we find the "true" growth yield $Y_{G,s}$ to be a decreasing function of growth rate, and therefore the specific bulk respiration $R_{b,s}$ is a nonlinear function of growth rate.

For the rDEB model, we can further derive a relationship between the maximum specific growth rate $\mu_{max,r}$ and the transformed specific

maintenance respiration rate $m_{q,r}$ as

$$\frac{\mu_{max,r}}{m_{q,r}} = \frac{c_1}{c_1 + c_2 a_{max,r}} \left(\frac{1 - f_{N,r}}{1 - Y_{RN,r} f_{N,r}} \frac{Y_{RV,r} a_{max,r}}{m_{V,r}} - 1 \right). \quad (54)$$

Similarly, for the sDEB model, we have

$$\frac{\mu_{max,s}}{m_{V,s}} = \frac{\kappa_s}{\kappa_s + Y_{RV,s} a_{max,s}} \left(\frac{Y_{RV,s} a_{max,s}}{m_{V,s}} - 1 \right). \quad (55)$$

In contrast, the tradeoff between $\mu_{max,c}$ and $m_{q,c}$ for the compromise model has to be prescribed if it is to be considered.

Moreover, by combing $Y_{G,r}$ in equation (47) and $R_{b,r}(S)$ in equation (40) for the rDEB model, and $Y_{G,s}$ in equation (53) and $R_{b,s}(S)$ in equation (50) for the sDEB model, the specific bulk respiration is found to be related with growth rate μ through the following form:

$$R_b(S) = \left(\frac{\theta_1}{1 - \theta_2 \mu} - 1 \right) \mu + \frac{\theta_3}{1 - \theta_2 \mu}, \quad (56)$$

where θ_1, θ_2, and θ_3 are positive parameters that can be estimated when equation (56) is applied to observations of specific bulk respiration R_b and specific growth rate μ.

From the equations in this section, we infer that (1) the compromise model is a reduced form of the sDEB model, while the sDEB model is a reduced form of the rDEB model; (2) the "true" growth yield $Y_{G,c}$ in the compromise model is an emergent parameter that should decrease with growth rate (as shown by its counterparts $Y_{G,r}$ in the rDEB model, and $Y_{G,s}$ in the sDEB model); (3) the linear relationship between the specific bulk respiration $R_{b,c}$ and specific growth rate μ_c predicted by the compromise model (equation (35)) is likely insufficient compared to the nonlinear relationship predicted by both DEB models (equation (56)), which will be further discussed in the next paragraph; and (4) the maximum growth rate $\mu_{max,c}$ and specific physiological maintenance respiration factor $m_{q,c}$ in the compromise model should be correlated as shown by both DEB models (equation (54) and (55)). In particular, if we consider that $a_{max,r}$ (or $a_{max,s}$) scales with surface area, and $m_{V,r}$ (or $m_{V,s}$) scales with volume, the ratio between maximum growth rate μ_{max} and physiological maintenance rate m_q can be inferred to decreases with cell size. However, it should be noted that under conditions where microbial elemental stoichiometry is changing dynamically, the relationship between μ_{max} and m_q is much more complicated and likely cannot be formulated analytically.

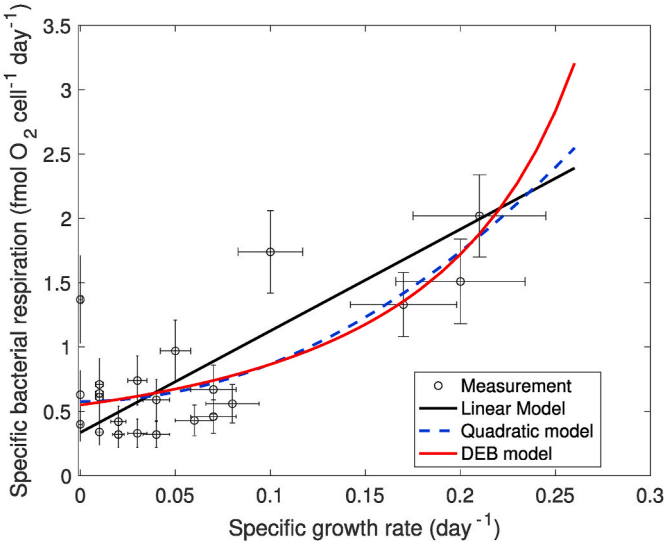

Fig. 2. Evaluation of three respiration-growth rate relationship models. The measurements are from Vikstrom and Wikner (2019), who collected bacterial cell-specific respiration rate and cell-specific growth rate for August from 11 stations in the Ore Estuary, north western Bothnian Sea. The model equations and their statistics are in Table 2. Note, all lines should stop at the maximum growth rate (which unfortunately is unknown from the measurements).

To illustrate point (3) above, we compared the relationship between specific bulk respiration and specific growth rate as predicted by the compromise model (equation (35)) and the DEB (equation (56)) models using measurements reported by Vikstrom and Wikner (2019), who collected bacterial cell-specific respiration rate and cell-specific growth rate from 11 stations in the Ore Estuary, north western Bothnian Sea. The relationship based on DEB models fits better to the observations than that based on the compromise model in terms of both R^2 and root mean square error (RMSE) (Fig. 2 and Table 2). Although the empirical quadratic relationship proposed by Vikstrom and Wikner (2019) fits the observations better than the DEB models (the third column of Table 2 and Fig. 2), it fails to predict that specific growth rate cannot increase to infinity, as does the compromise model (the linear model in Table 2; though a μ_{max} can be prescribed). In comparison, both DEB models predict that specific growth rate cannot increase to infinity, because (by equation (56)) as μ increases to infinity, R_b will encounter a singular point at $\mu = 1/\theta_2$, then become zero or even negative. However, due to the tradeoff between the maximum growth rate and maintenance respiration (described in equations (54) and (55)), μ will never reach $1/\theta_2$.

3.2. Modeling biodegradation of 2,4-dichlorophenoxyacetic acid

In this example, we apply the compromise, rDEB and sDEB models (see Table 3 for equations of the three models) to the time series data of cumulative CO_2 for the microbial degradation of herbicide 2,4-dichlorophenoxyacetic acid as measured by Estrella et al. (1993). We obtained the model parameters using the Markov chain Monte Carlo (MCMC) method with a Gaussian error function that measures the deviation of model predictions and measurements (Vrugt, 2016).

The compromise and rDEB models were found to fit the observed CO_2 time series with very similar numerical accuracy, and their corresponding time series of substrate and total microbial biomass are very similar (blue and orange lines in Fig. 3). In order to obtain similar goodness of fit to CO_2 time series, the sDEB model has to use much smaller initial microbial biomass (which is 1.3% of that for the compromise model and rDEB model). Accordingly, substrates were consumed much faster (red line vs other two lines in Fig. 3a) and microbial biomass peaked much earlier (by about 3 days; Fig. 3b) in the sDEB model. However, because there are no measurements to directly constrain the temporal evolution of either the substrates or microbial biomass, the three models can be considered equally successful in fitting the CO_2 time series. Nevertheless, these results indicate that the rDEB model is a good candidate for modeling such problems. (The compromise model is equally good for this specific problem with fewer parameters, though it is not as good as the rDEB model for the problem in section 3.1, nor for the tradeoff between substrate uptake rate and biomass yield in section 3.3)

3.3. The tradeoff between apparent substrate use efficiency and growth or substrate uptake rate for an exponentially growing bacterial population

Thermodynamic analyses of heat engines imply that a faster engine is of lower energy use efficiency, and the highest efficiency is achieved when the engine is in equilibrium with the environment (i.e., not working at all) (Feynman et al., 2011). Since a heat engine must be running to do work (i.e., producing power), energy use efficiency (as measured by the ratio between power produced and the rate of energy input) should first increase and then decrease with power. A more relatable example is that a car engine needs to be running to produce power to move the car. However, as the engine runs faster, heat dissipation becomes more significant, such that a smaller fraction of the burnt fuel is used to produce useful work. Therefore, between a

Table 2
Regression models corresponding to Fig. 2. The linear model is predicted by the compromise model (i.e., equation (35)), the empirical quadratic model was proposed by Vikstrom and Wikner (2019) based on empirical observation, and the DEB model is based on equation (56).

	Linear model	Quadratic model	DEB model
Symbolic equation	$R_b = \theta_1\mu + \theta_2$	$R_b = \theta_1\mu^2 + \theta_2$	$R_b = \left(\frac{\theta_1}{1-\theta_2\mu} - 1\right)\mu + \frac{\theta_3}{1-\theta_2\mu}$,
Best fit equation	$R_b = 7.91\mu + 0.34$, $R^2 = 0.45$, RMSE = 0.36	$R_b = 29.1\mu^2 + 0.58$, $R^2 = 0.58$, RMSE = 0.31	$R_b = \left(\frac{1.44}{1-2.82\mu} - 1\right)\mu + \frac{0.55}{1-2.82\mu}$, $R^2 = 0.58$, RMSE = 0.32
Parameter 95% confidence intervals	θ_1 : $[5.37, 10.4]$, θ_2 : $[0.194, 0.478]$	θ_1 : $[17.7, 40.6]$, θ_2 : $[0.411, 0.743]$	θ_1 : $[0.150, 4.40]$, θ_2 : $[1.23, 3.44]$, θ_3 : $[0.379, 0.687]$

Table 3
Equations for the three models used for the example problem of biodegradation of 2,4-dichlorophenoxyacetic acid in section 3.2. Note that here we adopted the same assumption in Estrella et al. (1993) that dead biomass is not contributing to growth during the experiment.

Compromise model	Equation for
$\frac{dS}{dt} = q_c(S)B_c$,	Substrate
$\frac{d\mathrm{CO_2}}{dt} = [q_c(S) - \mu_c(S)]B_c$,	CO_2
$\frac{dB_c}{dt} = (\mu_c(S) - \gamma_{M,c})B_c$,	Living biomass
$\frac{dB_{d,c}}{dt} = \gamma_{M,c}B_c$,	Dead biomass
sDEB model	**Equation for**
$\frac{dS}{dt} = \frac{a_{max,s}S}{K_{S,s}+S}\frac{X_{V,s}}{Y_{SR,s}}$,	Substrate
$\frac{d\mathrm{CO_2}}{dt} = \frac{a_{max,s}S}{K_{S,s}+S}X_{V,s}\left(\frac{1}{Y_{SR,s}} - 1\right) + R_{T,s}$,	CO_2
$\frac{dX_{R,s}}{dt} = \frac{a_{max,s}S}{K_{S,s}+S}X_{V,s} - (\kappa_s - g_{V,s} + \gamma_{M,s})X_{R,s}$,	Living reserve biomass
$\frac{dX_{V,s}}{dt} = (g_{V,s} - \gamma_{M,s})X_{V,s}$,	Living structural biomass
$\frac{dB_{d,s}}{dt} = [\gamma_M + max(0, -g_{V,s})](X_{V,s} + X_{R,s})$.	Total dead biomass
rDEB model	**Equation for**
$\frac{dS}{dt} = \frac{a_{max,r}S}{K_{S,r}+S}\frac{X_{V,r}}{Y_{SR,r}}$,	Substrate
$\frac{d\mathrm{CO_2}}{dt} = \frac{a_{max,r}S}{K_{S,r}+S}X_{V,r}\left(\frac{1}{Y_{SR,r}} - 1\right) + R_{T,r}$,	CO_2
$\frac{dX_{R,r}}{dt} = \frac{a_{max,r}S}{K_{S,r}+S}X_{V,r} - (\kappa_r - g_{V,r} + \gamma_{M,r})X_{R,r} + \frac{X_{N,r}}{\tau_{N,r}}$,	Living reserve biomass
$\frac{dX_{N,r}}{dt} = Y_{RN,r}f_{N,r}\kappa_r X_{R,r} - \frac{X_{N,r}}{\tau_{N,r}} + (g_{V,r} - \gamma_{M,r})X_{N,r}$,	Living kinetic biomass
$\frac{dX_{V,r}}{dt} = (g_{V,r} - \gamma_{M,r})X_{V,r}$,	Living structural biomass
$\frac{dB_{d,r}}{dt} = [\gamma_{M,r} + max(0, -g_{V,r})](X_{V,r} + X_{N,r} + X_{R,r})$.	Total dead biomass

zero-power-zero-efficiency static engine and a rapidly running engine that loses all its power through heat dissipation (resulting in zero efficiency), there is a point where the engine has maximum efficiency of fuel use to produce useful work. Such non-monotonic variation of energy use efficiency is well established in finite-time and control thermodynamics (Salamon et al., 2001; Roach et al., 2018). As a special type of heat engine driven by chemical energy, we thus expect a biological organism to first increase its apparent substrate use efficiency (defined as the ratio between specific growth rate $\mu(S)$ and specific substrate uptake rate $q(s)$) and then decrease it with increasing growth rate. The *apparent substrate use efficiency* here has been termed 'substrate-use efficiency' or 'carbon-use efficiency' (when carbon is the substrate) in many other studies, e.g., Bolscher et al. (2017), Qiao et al. (2019). Nonetheless, we recognize that, for an organism, substrate use from uptake to structural biomass construction involves multiple steps, particularly when the organism is represented with the DEB models (where newly assimilated substrate may be stored as reserve biomass and used later for microbial metabolism). Consequently, the use efficiency of a substrate for an organism is an emergent parameter that depends on the physiological status of the organism and is generally a function of time. Therefore, we term it 'apparent substrate use efficiency' to emphasize its dynamic nature. It is noted that, when applied to carbon, the inferences here and below are valid for the 'apparent carbon use efficiency'. However, even though the emergent tradeoff functions derived from the DEB models are better at providing mechanistic interpretations to the empirical data than existing empirical models (as we will see below), they are not recommended to be used directly to model microbial dynamics under general conditions.

For the compromise model, we have its apparent substrate use efficiency ($Y_{app,c}$) as

$$Y_{app,c} = \frac{\mu_c}{q_c} = \frac{\mu_c}{\mu_c + m_{q,c}}Y_{G,c}. \tag{57}$$

For the sDEB model, we have

$$Y_{app,s} = \frac{\mu_s}{q_s} = \frac{\mu_s}{\mu_s + m_{V,s}}\left(1 - \frac{\mu_s}{\kappa_s}\right)Y_{SR,s}Y_{RV,s}. \tag{58}$$

And for the rDEB model, we have

$$Y_{app,r} = \frac{\mu_r}{q_r} = \frac{\mu_r}{\mu_r + m_{q,r}}\left(\frac{1 - f_{N,r}}{1 - Y_{RN,r}f_{N,r}} - c_2\mu_r\right)\frac{Y_{SR,r}}{c_1}, \tag{59}$$

For equation (59), if we take the approximation $c_1 = 1/Y_{RV,r}$ (since $K_{R,r} < 10^{-10}$ under normal conditions as shown in section A in the supplemental material), and $c_2 = 1/[(1 - Y_{RN,r}f_{N,r})\kappa_s]$ (by neglecting the first term in the braces of equation (B30) in section B of the supplemental material), $Y_{app,r}$ becomes

$$Y_{app,r} = \frac{\mu_r}{\mu_r + m_{V,r}}\left(\frac{1 - f_{N,r}}{1 - Y_{RN,r}f_{N,r}} - \frac{\mu_r}{(1 - Y_{RN,r}f_{N,r})\kappa_s}\right)Y_{SR,r}Y_{RV,r}, \tag{60}$$

Additionally, (as derived in supplemental material D), we can relate the apparent substrate use efficiency to specific substrate uptake rate for the compromise model

$$Y_{app,c} = Y_{G,C}\left(1 - \frac{m_{q,c}/Y_{G,C}}{q_c}\right), \tag{61}$$

for the sDEB model

$$Y_{app,s} = \frac{q_s - m_{V,s}/Y_o}{q_s(1 + Y_{SR,s}Y_{RV,s}q_s/\kappa_s)}Y_{SR,s}Y_{RV,s}, \tag{62}$$

and for the rDEB model

$$Y_{app,r} = \frac{1}{q(1 + Y_{SR,r}Y_{RV,r}q/[(1 - Y_{RN,r}f_{N,r})\kappa_s])}\left(q\frac{1 - f_{N,r}}{1 - Y_{RN,r}f_{N,r}} - \frac{m_{V,r}}{Y_{SR,r}Y_{RV,r}}\right)Y_{SR,r}Y_{RV,r}, \tag{63}$$

From equation (57) and the blue line in Fig. 4a, we observe that, in the compromise model, the apparent substrate use efficiency is an increasing function of growth rate, which is inconsistent with thermodynamic theory. In contrast, both sDEB and rDEB models (equation (58)

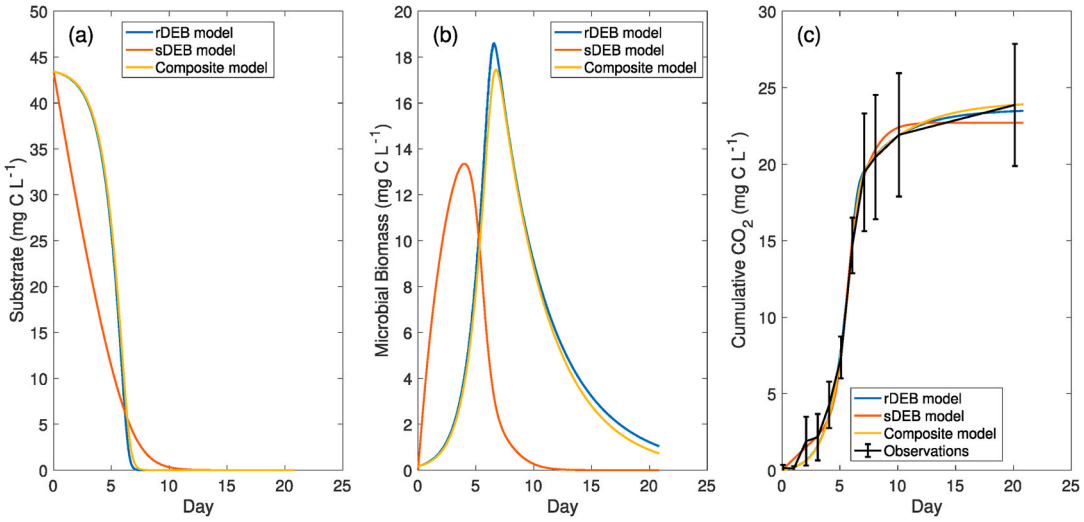

Fig. 3. Comparsion of the best fitting of three models for simulating the degradation of the herbicide *2,4-dichlorophenoxyacetic acid.* (a) Evolution of substrate, (b) evolution of microbial biomass, and (c) evolution of cumulative CO_2. Model parameters are shown in Table S1 of the supplemental material. For the sDEB model, the initial biomass is about 1.3% of that for the compromise model, with 29.4% as structural biomass and 70.6% as reserve biomass, respectively; for the rDEB model, the initial biomass is the same as for the compromise model, with 28% as structural biomass, 6% as reserve biomass, and 66% as kinetic biomass, respectively. The biomass for different compartments of the DEB models is shown in Fig. S1 of the supplemental material.

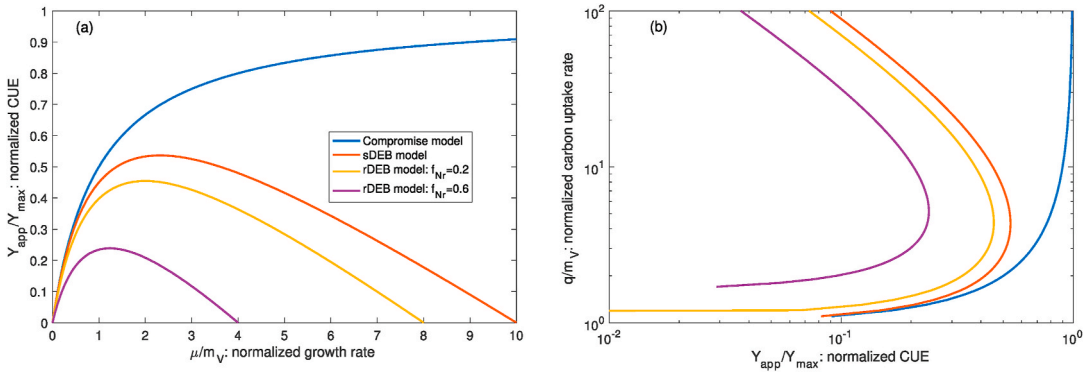

Fig. 4. (a) Tradeoff between the apparent substrate use efficiency Y_{app} (normalized by its maximum value Y_{max}) and the growth rate μ (normalized by structural maintenance respiration m_V) for the three models. (b) Tradeoff between the specific substrate uptake rate (normalized by structural maintenance respiration m_V) and the apparent substrate use efficiency Y_{app} (normalized by its maximum value Y_{max}). For the compromise model, $Y_{max} = Y_{G,c}$, and $m_V = m_q$, respectively. For the sDEB model, $Y_{max} = Y_{SR,s}Y_{RV,s}$, and $m_V = m_{V,s}$ respectively. For the rDEB model, $Y_{max} = Y_{SR,r}Y_{RV,r}$ and $m_V = m_{V,r}$ respectively. For the rDEB model in (a), the results are plotted using equation (60) for simplicity. Both DEB models assume $\kappa_x/m_V = 10$, with x as r and s for rDEB and sDEB models, respectively (and a different ratio does not change the results qualitatively).

and (60), and non-blue lines in Fig. 4a) infer that the apparent substrate use efficiency first increases and then decreases as a function of growth rate, which agrees with thermodynamic theory and is supported by a synthesis of large sets of empirical data (Lipson, 2015). The increase of apparent substrate use efficiency is driven by the increase of power for growth (assuming the cost for maintaining structural biomass is relatively constant) when the organism is substrate limited, while the decrease of apparent substrate use efficiency at high growth rate is due to the dilution effect of reserve density (which can be understood as an increase in entropy due to the increased intracellular space explored by the growing microbial biomass). For instance, in the sDEB model, the increase of structural biomass $X_{V,s}$ diminishes the reserve biomass density ($X_{R,s}/X_{V,s}$), as manifested by term $-g_{V,s}X_{R,s}$ in equation (3), making it increasingly more difficult to maintain the high metabolic rate at a higher growth rate. In this sense, mechanisms like overflow metabolism, futile cycles, and increased protein synthesis costs, as proposed in Lipson (2015), are all part of the thermodynamic necessity accompanying the increase in intracellular volume resulting from growth. The overflow metabolism can be accompanied by changes in proteomic allocations to different metabolic pathways (Basan et al., 2015), which could also be driven by the stoichiometric necessity if nutrients are limiting (Salar-Garcia et al., 2017). Additionally, the dilution effect imposes a maximum growth rate κ_s (the specific reserve mobilization rate), which in the rDEB model is determined by intracellular enzyme kinetics (i.e., κ_r in equation (12)) that are a function of the associated microbial proteomics (Zeng and Yang, 2020), and is accounted for with parameter $f_{N,r}$ in equation (59).

Following equation (61) for the compromise model, the substrate uptake rate is positively correlated with the apparent substrate use efficiency (Fig. 4b). In contrast, the DEB models (equation (62) and (63)) show a non-monotonic relationship, i.e., a given apparent substrate use efficiency can be realized at both a low and high specific substrate uptake rate (non-blue lines in Fig. 4b). In particular, the non-monotonic relationship revealed by the DEB models qualitatively better agree with the synthesis data in Fig. 4B of Calabrese et al. (2021) (which was based on the 132 experiments synthesized by Smeaton and Van Cappellen (2018)), where they inferred that specific substrate uptake rate decreases linearly with the apparent substrate use efficiency (i.e.

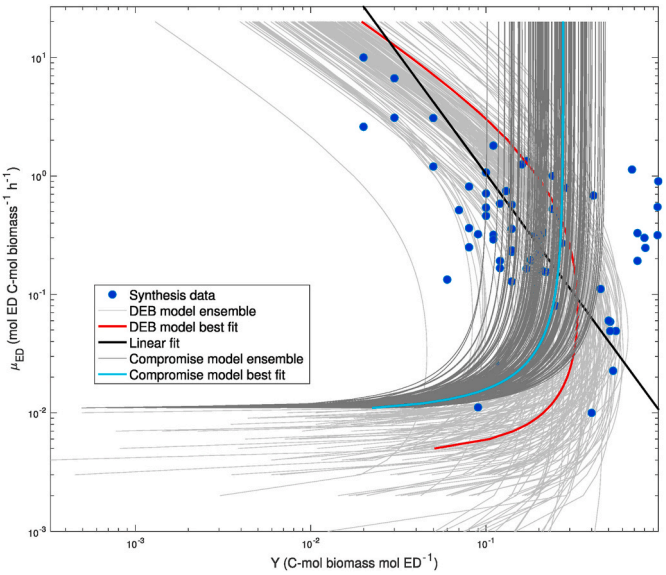

Fig. 5. Evaluation of the DEB model (i.e., equation (64)) and compromise model (i.e., equation (61)) predicted tradeoff between specific substrate uptake rate and biomass yield using the synthesis data from Smeaton and Van Cappellen (2018). Ensemble lines are drawn for the Bayesian posterior model parameters inferred with the MCMC method (Vrugt, 2016). The black solid line is predicted from the power law model by Calabrese et al. (2021). In the 10-base log space, the DEB model best fit has a regression with measured biomass yield of $y = 1.22x + 0.006$, RMSE = 0.33, $R^2 = 0.36$; the power law model has $y = 0.69x - 0.23$, RMSE = 0.36, $R^2 = 0.25$; and the compromise model has $y = -0.13x - 0.85$, RMSE = 0.41, $R^2 = 0.01$; with y being log10 of measured biomass yield, and x being log10 of model predicted biomass yield. Fitted model parameters are in Table S2.

biomass yield in their terminology) in the 10-base loglog space (i.e., a power law between substrate uptake rate and the apparent substrate use efficiency; see their equations (6) and (7) and black line in Fig. 5), even though there are evidently both high and low substrate uptake rates realizing the same apparent substrate use efficiency (e.g., blue dots in Fig. 5). This indicates that a relationship derived from the DEB models:

$$Y_{app} = \frac{q\vartheta_1 - m/Y_o}{q(1 + \vartheta_2 Y_o q)} Y_o \tag{64}$$

is likely a better choice to interpret their data (with parameters ϑ_1, ϑ_2, m and Y_O). Indeed, when equation (64) is used to fit the tradeoff between substrate uptake rate and biomass yield synthesized by Smeaton and Van Cappellen (2018), more variability of the tradeoff is explained than the empirical power law model proposed by Calabrese et al. (2021). Particularly, equation (64) explains that a relatively low biomass yield may correspond to both high and low substrate uptake rates (red and light gray lines in Fig. 5). However, because the synthesis data covers diverse bacteria that harvest Gibbs energy using different redox pairs (and some experiments may even not meet the criteria of the assumed exponential growth), one should not be surprised to see that even equation (64) fails to fit all the data points. Lastly, the compromise model is not able to explain the majority of the synthesis data, and is valid likely only in the low substrate uptake rate regime (cyan line and dark gray lines in Fig. 5).

In summary, one important conclusion from this comparison of apparent substrate use efficiency dynamics among the two DEB models and two empirical models (i.e., the compromise and power law models) is that a thermodynamically consistent modeling of biological growth requires growth to be a function of cellular quota of relevant nutrients (adopting Droop's broader definition of nutrients which includes carbon (Droop, 1974; Cherif and Loreau, 2010)). Among existing models, DEB models and Droop models (Droop, 1974) adopted such a strategy (and it can be shown that Droop models predict that apparent substrate use efficiency decreases with growth rate, thus failing to resolve the non-monotonic tradeoff), while the compromise and Monod models that formulate growth as a function of external substrate concentration are not able to resolve the substrate use efficiency dynamics properly (even though the compromise model can account for the initial increase of substrate use efficiency with growth rate (Beeftink et al., 1990)). Additionally, we note that for a non-exponentially growing microbial population, because the reserve biomass density (and the kinetic biomass density for the rDEB model) are not in steady state, the dynamics of apparent substrate use efficiency simulated by DEB models are much more complicated (such as shown in Tang and Riley (2015) for the substrate use efficiency relationship with temperature). Finally, because these inferences are made based on generic principles, they should be applicable to both individuals and populations of microbes.

4. Discussion

4.1. Improved predictability of DEB models compared to empirically based models

Our model evaluation with empirical data in section 3 indicates that DEB models are more accurate than the empirically based models for describing tradeoffs among biogeochemical variables, such as that between bulk specific respiration and specific growth rate, and between apparent substrate use efficiency and specific growth rate (or specific substrate uptake rate). We attribute these improvements to the scaling coherency built into the DEB models, particularly for the rDEB model, which links the law of mass action (which can be rigorously derived from thermodynamics and statistical mechanics, rooted in Newton's laws, and conservation laws for mass, energy, momentum, etc. (Pauli, 1973)) to growth dynamics. In contrast, empirical models (which are used by most published modeling studies) are often limited by data availability, and the assumed functional forms used in parametric fitting. In particular, to be parsimonious, simple functional forms with fewer parameters are preferred (and reasonably complex functional forms are difficult to guess). (Thus, in some sense, developing empirical models are like machine learning without physics guidance, and accounting for physical constraints is recently found critical for the success of machine learning (Zhao et al., 2019; Zhu et al., 2019b).) These limitations often force empirical functions to regard potentially meaningful data variability as model noise, so that the resultant models have exaggerated the model sensitivity to certain forcing variables (e.g., temperature (Tang and Riley, 2015)), and demonstrate less spatiotemporal variability than observations (one outstanding issue that is plaguing the predictive power of existing biogeochemical models; Carvalhais et al. (2014)). We thus advocate that more efforts should be devoted to develop theories like DEB models that better account for biogeochemical tradeoffs through incorporation of mechanistic processes and conservation laws that support the explanatory and predictive successes of physics (Feynman, 2017).

4.2. Potential extension to include proteomic control of biological growth modeling

One improvement of the rDEB model over both the sDEB and the compromise models is that the rDEB model can account for the tradeoff between metabolic activity (that is equivalent to reserve biomass turnover rate) and (structural biomass) growth as a function of ribosomes allocated for synthesizing metabolic enzymes (which are a major component of kinetic biomass) versus growth of structural biomass. This tradeoff manifests as the maximum growth rate decreasing with the fraction of mobilized reserve biomass allocated to kinetic biomass synthesis ($f_{N,r}$, Fig. 6). However, the rDEB model predicts that the greatest maximum growth rate occurs when $f_{N,r} = 0$, a condition which implies zero kinetic biomass and consequently zero turnover of reserve biomass.

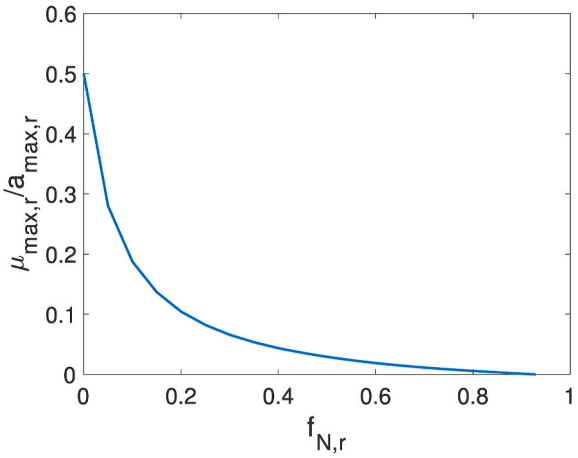

Fig. 6. Normalized maximum growth rate as a function of $f_{N,r}$ (the fraction of mobilized reserve biomass allocated to kinetic biomass synthesis) as derived by equation (41).

Since the sDEB model can be derived from the rDEB model with $f_{N,r} = 0$, the sDEB model should, paradoxically, have zero growth rate. Further, since microbes can adjust their proteomics to the environment, under steady substrate supply, there is an f_{N*} whose proteomic condition maximizes the growth rate, so that a monotonic curve as shown in Fig. 6 cannot exist. This assertion can be shown with the following argument: if $f_{N,r}$ corresponding to the current proteomics is not maximizing the growth rate for the given substrate supply, then by their physiological plasticity, microbes with f_{N*} corresponding to a new proteomic distribution will outcompete microbes with other values of $f_{N,r}$. These two inferences suggest that (1) the rDEB model should be modified to better represent the proteomic control of microbial growth; (2) the sDEB model, as a limiting case of the rDEB model, may not accurately simulate microbial physiology, and (3) neither the rDEB nor sDEB models are sufficient to support genome-informed microbial modeling of microbial physiology, even though they both are superior to the compromise model (which is parent to many other model formulations in the literature (Picioreanu et al., 2000; Moussa et al., 2005; Wang and Post, 2012)) in describing the relationship between bulk respiration and growth rate, and the relationship between apparent substrate use efficiency and growth rate (or substrate uptake rate).

We suggest that future work can incorporate proteomic controls on microbial physiology by (1) further dividing the kinetic biomass compartment into at least two compartments: one for catabolic enzymes (to produce energy from reserve biomass) and the other for ribosomes (to synthesize proteins to support the production of kinetic biomass and structural biomass compartments), and (2) defining $f_{N,r}$ as the allocation of ribosomes used for kinetic biomass. With this design, one equation can be obtained for the catabolic activity and another equation for the anabolic activity, with $f_{N,r}$ and growth rate as two unknowns. Therefore, the solution f_{N*} to these two equations gives the greatest maximum growth rate that can be achieved for a given external substrate supply (as other solutions will either lead to a deficit in catabolic energy or shortage in reserve flux for anabolism).

5. Conclusions

By partitioning the biomass into reserve, kinetic, and structural compartments, and invoking the Equilibrium Chemistry Approximation kinetics for reserve mobilization, we revised the dynamic energy budget model for simulating microbial physiological dynamics. The rDEB (revised DEB) model includes the sDEB (standard DEB) model as a special case, and they both predict that emergent microbial substrate (including carbon) use efficiency first increases and then decreases with growth rate. Further, their predicted relationships between microbial respiration and growth rate better explained a dataset of marine microbial respiration collected by Vikstrom and Wikner (2019). They also better explained the synthesis data on the substrate uptake rate and growth yield tradeoff by Smeaton and Van Cappellen (2018). The DEB models can also be reduced to the popular compromise model, which is parent to some other microbial models (Picioreanu et al., 2000; Moussa et al., 2005). The DEB models predict that the maximum growth rate and physiological maintenance factor in the compromise model are negatively correlated, a tradeoff that implies a cell-size regulation on microbial growth. However, the rDEB model predicts no optimal allocation for ribosome effort (as proportional to the kinetic biomass) for synthesizing kinetic biomass and structural biomass. This shortcoming suggests that biomass should be partitioned into at least four compartments to represent proteomic control on biological growth, potentially bridging the gap between phenological growth models and flux-balance based models. We expect further modifications to the rDEB model will allow tradeoffs in microbial physiology to be dynamically predicted rather than imposed for many applications.

Table A
Nomenclature.

Symbol	Unit	Meaning
$a_{max,r}$	s^{-1}	Maximum substrate assimilation rate for the rDEB model.
$a_{max,s}$	s^{-1}	Maximum substrate assimilation rate for the sDEB model.
c_1	None	Intermediate variable for the rDEB model.
c_2	s	Intermediate variable for the rDEB model.
d_N	None	Ratio of mass density of structural biomass to that of non-structural biomass in the rDEB model.
d_R	None	Ratio of mass density of structural biomass to that of reserve biomass in the rDEB model.
$f_{N,r}$	None	Fraction of mobilized reserve flux used for kinetic biomass synthesis in the rDEB model.
$g_{V,r}$	s^{-1}	Specific growth rate for the rDEB model.
$g_{V,s}$	s^{-1}	Specific growth rate for the sDEB model.
$h(S)$	None	Functional response to substrate availability for the compromise model.
$\overline{h}_r(S)$	None	Functional response to substrate availability for the rDEB model.
$\overline{h}_s(S)$	None	Functional response to substrate availability for the sDEB model.
$j_{A,r}$	s^{-1}	Specific substrate assimilation flux for the rDEB model.
$j_{A,s}$	s^{-1}	Specific substrate assimilation flux for the sDEB model.
$j_{RN,r}$	s^{-1}	Specific reserve mobilization rate for rDEB model
m_q	s^{-1}	Physiological maintenance coefficient for the compromise model.
$m_{q,r}$	s^{-1}	Transformed physiological maintenance coefficient for the rDEB model.
$m_{V,r}$	s^{-1}	Physiological maintenance coefficient for the rDEB model.
$m_{V,s}$	s^{-1}	Physiological maintenance coefficient for the sDEB model.
q_c	s^{-1}	Specific substrate uptake rate for the compromise model.
q_r	s^{-1}	Specific substrate uptake rate for the rDEB model.
q_s	s^{-1}	Specific substrate uptake rate for the sDEB model.
$v_{max,j}$	s^{-1}	Maximum process rate of substrate S_j.
$x_{N,r}$	None	kinetic biomass density for the rDEB model.
$x_{R,r}$	None	Reserve biomass density for the rDEB model
$x_{R,s}$	None	Reserve biomass density for the sDEB model
A	None	Intermediate variable for the rDEB model.
B_c	mg C $liter^{-1}$	Microbial biomass for the compromise model applied in Fig. 3.
$B_{d,r}$	mgC $liter^{-1}$	Dead microbial biomass for the rDEB model applied in Fig. 3.
$B_{d,s}$	mgC $liter^{-1}$	Dead microbial biomass for the sDEB model applied in Fig. 3.
D_E	$m^2\ s^{-1}$	Enzyme diffusivity (relative to substrate) in the cytosol.
E	gC m^{-3}	Enzyme concentration.
F_j	mol m^{-3} s^{-1}	Consumption flux of substrate S_j.
F	mol m^{-3} s^{-1}	Sum of F_j.
$J_{A,r}$	gC $m^{-3}s^{-1}$	Substrate assimilation flux
$J_{A,s}$	gC $m^{-3}s^{-1}$	Substrate assimilation flux

(*continued on next page*)

Table A (*continued*)

Symbol	Unit	Meaning
$J_{RN,r}$	gC m^{-3} s^{-1}	Gross reserve mobilization flux for the rDEB model.
$J_{RN,r,1}$	gC m^{-3} s^{-1}	Reserve mobilization flux goes to kinetic biomass in the rDEB model.
$J_{RN,r,2}$	gC m^{-3} s^{-1}	Reserve mobilization flux goes to structural biomass in the rDEB model.
K_j	mol m^{-3}	Dissociation parameter between enzyme E and substrate S_j.
$K_{R,r}$	None	Dissociation parameter between reserve and non-structural biomass in the rDEB model.
K_S	gC m^{-3}	Dissociation parameter between microbes and substrate S.
$\overline{K}_{S,r}$	gC m^{-3}	Transformed dissociation parameter between microbes and substrate S for the rDEB model.
$\overline{K}_{S,s}$	gC m^{-3}	Transformed dissociation parameter between microbes and substrate S for the sDEB model.
$R_{b,c}$	s^{-1}	Specific bulk respiration for the compromise model.
$R_{b,r}$	s^{-1}	Specific bulk respiration for the rDEB model.
$R_{b,s}$	s^{-1}	Specific bulk respiration for the sDEB model.
$R_{T,r}$	gC m^{-3} s^{-1}	Total respiration for the rDEB model.
$R_{T,s}$	gC m^{-3} s^{-1}	Total respiration for the sDEB model.
$R_{M,r}$	gC m^{-3} s^{-1}	Total respiration associated with reserve mobilization in the rDEB model.
$R_{M,s}$	gC m^{-3} s^{-1}	Total respiration associated with reserve mobilization in the sDEB model.
S	gC m^{-3} s^{-1}	Substrate
$X_{N,r}$	gC m^{-3}	kinetic biomass for the rDEB model.
$X_{R,r}$	gC m^{-3}	Reserve biomass for the rDEB model.
$X_{R,s}$	gC m^{-3}	Reserve biomass for the sDEB model.
$X_{V,r}$	gC m^{-3}	Structural biomass for the rDEB model.
$X_{V,s}$	gC m^{-3}	Structural biomass for the sDEB model.
$Y_{app,c}$	None	Apparent substrate use efficiency for the compromise model.
$Y_{app,r}$	None	Apparent substrate use efficiency for the rDEB model.
$Y_{app,s}$	None	Apparent substrate use efficiency for the sDEB model.
$Y_{G,c}$	None	Apparent biomass yield rate for the compromise model
$Y_{G,r}$	None	Apparent biomass yield rate for the rDEB model.
$Y_{G,s}$	None	Apparent biomass yield rate for the sDEB model.
$Y_{RN,r}$	None	Conversion coefficient from reserve to kinetic biomass in the rDEB model.
$Y_{RV,r}$	None	Conversion coefficient from reserve to structural biomass in the rDEB model.
$Y_{RV,s}$	None	Conversion coefficient from reserve to structural biomass in the sDEB model.
$Y_{SR,r}$	None	Conversion coefficient from substrate to reserve biomass in the sDEB model.
$Y_{SR,s}$	None	Conversion coefficient from substrate to reserve biomass in the rDEB model.
α_r	None	Binding scaling coefficient between reserve and kinetic biomass in the rDEB model.
$\gamma_{M,c}$	s^{-1}	Specific mortality rate for the compromise model.
$\gamma_{M,r}$	s^{-1}	Specific mortality rate for the rDEB model.
$\gamma_{M,s}$	s^{-1}	Specific mortality rate for the sDEB model.
μ_c	s^{-1}	Specific growth rate for the compromise model.
$\mu_{max,c}$	s^{-1}	Maximum specific growth rate for the compromise model
μ_r	s^{-1}	Specific growth rate for the rDEB model.
μ_s	s^{-1}	Specific growth rate for the sDEB model.
$\mu_{max,r}$	s^{-1}	Maximum specific growth rate for the rDEB model
$\mu_{max,s}$	s^{-1}	Maximum specific growth rate for the sDEB model.
σ	None	Shape parameter for intracellular tortuosity in the rDEB model.
ε	Pa	Elasticity of the cell wall.
Π_0	Pa	Turgor pressure at full turgor
Π	Pa	Turgor pressure
$\tau_{N,r}$	s-1	Turnover time of kinetic biomass in the rDEB model.
κ_r	s-1	Specific reserve biomass turnover rate for rDEB model
κ_s	s-1	Specific reserve biomass turnover rate for sDEB model
$\kappa_{max,r}$	s^{-1}	Maximum value of κ_r
φ_V	None	Cellular space taken up by structural biomass
φ_N	None	Intracellular space taken up by one unit of non-structural biomass
φ_R	None	Intracellular space taken up by one unit of reserve biomass

Declaration of competing interest

The authors declare the following financial interests/personal relationships which may be considered as potential competing interests: Jinyun Tang reports financial support was provided by US Department of Energy. William J. Riley reports financial support was provided by US Department of Energy.

Data availability

Only published data were used.

Acknowledgements

This research was supported by the Director, Office of Science, Office of Biological and Environmental Research of the US Department of Energy under contract no. DE-AC02-05CH11231 as part of the Belowground Biogeochemistry SFA and the Next Generation Ecosystem Experiment-Arctic project. Financial support does not constitute an endorsement by the Department of Energy of the views expressed in this study. The authors declare no conflicts of interest. We sincerely appreciate the suggestions given by the two anonymous reviewers and the handling editor Stefano Manzoni. They helped us improve the manuscript from its earlier versions significantly.

Appendix A. Supplementary data

Supplementary data related to this article can be found at https://doi.org/10.1016/j.soilbio.2023.108954.

References

Apostol, T.M., 1967. Calculus, 2d, ed. Blaisdell, Waltham, Massachusetts.
Barnum, T.P., Cheng, Y.W., Hill, K.A., Lucas, L.N., Carlson, H.K., Coates, J.D., 2020. Identification of a parasitic symbiosis between respiratory metabolisms in the biogeochemical chlorine cycle. The ISME Journal 14, 1194–1206.
Basan, M., Hui, S., Okano, H., Zhang, Z.G., Shen, Y., Williamson, J.R., Hwa, T., 2015. Overflow metabolism in Escherichia coli results from efficient proteome allocation. Nature 528, 99–104.
Beeftink, H.H., Vanderheijden, R.T.J.M., Heijnen, J.J., 1990. Maintenance requirements - energy supply from simultaneous endogenous respiration and substrate consumption. FEMS Microbiology Ecology 73, 203–209.
Bolscher, T., Paterson, E., Freitag, T., Thornton, B., Herrmann, A.M., 2017. Temperature sensitivity of substrate-use efficiency can result from altered microbial physiology without change to community composition. Soil Biology and Biochemistry 109, 59–69.
Calabrese, S., Chakrawal, A., Manzoni, S., Van Cappellen, P., 2021. Energetic Scaling in Microbial Growth, vol. 118. Proceedings of the National Academy of Sciences of the United States of America.
Carvalhais, N., Forkel, M., Khomik, M., Bellarby, J., Jung, M., Migliavacca, M., Mu, M.Q., Saatchi, S., Santoro, M., Thurner, M., Weber, U., Ahrens, B., Beer, C., Cescatti, A., Randerson, J.T., Reichstein, M., 2014. Global covariation of carbon turnover times with climate in terrestrial ecosystems. Nature 514, 213.
Chebotareva, N.A., Kurganov, B.I., Livanova, N.B., 2004. Biochemical effects of molecular crowding. Biochemistry-Moscow 69, 1239–1251.
Cheng, Y.W., Bouskill, N.J., Brodie, E.L., 2019. Model exploration of interactions between algal functional diversity and productivity in chemostats to represent open ponds systems across climate gradients. Ecological Modelling 406, 121–132.
Cherif, M., Loreau, M., 2010. Towards a more biologically realistic use of Droop's equations to model growth under multiple nutrient limitation. Oikos 119, 897–907.
Chowdhury, A., Zomorrodi, A.R., Maranas, C.D., 2014. K-OptForce: integrating kinetics with flux balance analysis for strain design. PLoS Computational Biology 10.
Ciliberto, A., Capuani, F., Tyson, J.J., 2007. Modeling networks of coupled enzymatic reactions using the total quasi-steady state approximation. PLoS Computational Biology 3, 463–472.
Dawes, E.A., Ribbons, D.W., 1962. The endogenous metabolism of microorganisms. Annual Review of Microbiology 16, 241–264.
Dix, J.A., Verkman, A.S., 2008. Crowding effects on diffusion in solutions and cells. Annual Review of Biophysics 37, 247–263.
Droop, M.R., 1974. Nutrient status of algal cells in continuous culture. Journal of the Marine Biological Association of the United Kingdom 54, 825–855.
Estrella, M.R., Brusseau, M.L., Maier, R.S., Pepper, I.L., Wierenga, P.J., Miller, R.M., 1993. Biodegradation, sorption, and transport of 2,4-dichlorophenoxyacetic acid in saturated and unsaturated soils. Applied and Environmental Microbiology 59, 4266–4273.

Etienne, T.A., Cocaign-Bousquet, M., Ropers, D., 2020. Competitive effects in bacterial mRNA decay. Journal of Theoretical Biology 504.
Feynman, R.P., 2017. The Character of Physical Law. The MIT Press.
Feynman, R.P., Leighton, R.B., Sands, M., 2011. The feynman lectures on physics. The New Millennium Edition. In: Mainly Mechanics, Radiation, and Heat, Edition, vol. I. Basic Books, New Millennium.
Hill, T.L., 1987. Statistical Mechanics: Principles and Selected Applications. Dover Publications.
Kempes, C.P., van Bodegom, P.M., Wolpert, D., Libby, E., Amend, J., Hoehler, T., 2017. Drivers of bacterial maintenance and minimal energy requirements. Frontiers in Microbiology 8.
Kempes, C.P., Wang, L., Amend, J.P., Doyle, J., Hoehler, T., 2016. Evolutionary tradeoffs in cellular composition across diverse bacteria. The ISME Journal 10, 2145–2157.
Kooijman, S.A.L.M., 2009. Dynamic Energy Budget Theory for Metabolic Organisation. Cambridge University Press, Cambridge.
Labhsetwar, P., Cole, J.A., Roberts, E., Price, N.D., Luthey-Schulten, Z.A., 2014. Heterogeneity in protein expression induces metabolic variability in a modeled Escherichia coli population (vol 110, pg 14006, 2013). Proceedings of the National Academy of Sciences of the United States of America 111, 876-876.
Labhsetwar, P., Melo, M.C.R., Cole, J.A., Luthey-Schulten, Z., 2017. Population FBA predicts metabolic phenotypes in yeast. PLoS Computational Biology 13.
Lipson, D.A., 2015. The complex relationship between microbial growth rate and yield and its implications for ecosystem processes. Frontiers in Microbiology 6.
Madigan, M.T., Martinko, J.M., Dunlap, P.V., Clark, D.P., 2009. Brock Biology of Microorganisms, twelfth ed. Pearson Eduction, Inc. , 1301 Sansome Street, San Francisco, CA 94111.
Milo, R., Phillips, R., 2015. Cell Biology by the Numbers, first ed. Garland Science.
Minton, A.P., 1990. Holobiochemistry - the effect of local environment upon the equilibria and rates of biochemical reactions. International Journal of Biochemistry 22, 1063–1067.
Minton, A.P., 1998. Molecular crowding: analysis of effects of high concentrations of inert cosolutes on biochemical equilibria and rates in terms of volume exclusion. Energetics of Biological Macromolecules, Pt B 295, 127–149.
Moldrup, P., Olesen, T., Komatsu, T., Yoshikawa, S., Schjonning, P., Rolston, D.E., 2003. Modeling diffusion and reaction in soils: X. A unifying model for solute and gas diffusivity in unsaturated soil. Soil Science 168, 321–337.
Monod, J., 1949. The growth of bacterial cultures. Annual Review of Microbiology 3, 371–394.
Moussa, M.S., Hooijmans, C.M., Lubberding, H.J., Gijzen, H.J., van Loosdrecht, M.C.M., 2005. Modelling nitrification, heterotrophic growth and predation in activated sludge. Water Research 39, 5080–5098.
Pauli, W., 1973. Statistical Mechanics. Dover Publications, Inc.
Picioreanu, C., van Loosdrecht, M.C.M., Heijnen, J.J., 2000. Effect of diffusive and convective substrate transport on biofilm structure formation: a two-dimensional modeling study. Biotechnology and Bioengineering 69, 504–515.
Pirt, S.J., 1965. Maintenance energy of bacteria in growing cultures. Proceedings of the Royal Society Series B-Biological Sciences 163, 224–231.
Pirt, S.J., 1982. Maintenance energy - a general-model for energy-limited and energy-sufficient growth. Archives of Microbiology 133, 300–302.
Qiao, Y., Wang, J., Liang, G.P., Du, Z.G., Zhou, J., Zhu, C., Huang, K., Zhou, X.H., Luo, Y. Q., Yan, L.M., Xia, J.Y., 2019. Global variation of soil microbial carbon-use efficiency in relation to growth temperature and substrate supply. Scientific Reports 9.
Roach, T.N.F., Salamon, P., Nulton, J., Andresen, B., Felts, B., Haas, A., Calhoun, S., Robinett, N., Rohwer, F., 2018. Application of finite-time and control thermodynamics to biological processes at multiple scales. Journal of Non-Equilibrium Thermodynamics 43, 193–210.
Salamon, P., Nulton, J.D., Siragusa, G., Andersen, T.R., Limon, A., 2001. Principles of control thermodynamics. Energy 26, 307–319.
Salar-Garcia, M.J., Bernal, V., Pastor, J.M., Salvador, M., Argandona, M., Nieto, J.J., Vargas, C., Canovas, M., 2017. Understanding the interplay of carbon and nitrogen supply for ectoines production and metabolic overflow in high density cultures of Chromohalobacter salexigens. Microbial Cell Factories 16.
Smeaton, C.M., Van Cappellen, P., 2018. Gibbs energy dynamic yield method (GEDYM): predicting microbial growth yields under energy-limiting conditions. Geochimica et Cosmochimica Acta 241, 1–16.
Song, H.S., Ramkrishna, D., 2011. Cybernetic models based on lumped elementary modes accurately predict strain-specific metabolic function. Biotechnology and Bioengineering 108, 127–140.
Steudle, E., Zimmermann, U., Luttge, U., 1977. Effect of turgor pressure and cell-size on wall elasticity of plant-cells. Plant Physiology 59, 285–289.
Tadmor, A.D., Tlusty, T., 2008. A coarse-grained biophysical model of E. coli and its application to perturbation of the rRNA operon copy number. PLoS Computational Biology 4.
Tang, J.Y., Riley, W.J., 2013. A total quasi-steady-state formulation of substrate uptake kinetics in complex networks and an example application to microbial litter decomposition. Biogeosciences 10, 8329–8351.
Tang, J.Y., Riley, W.J., 2015. Weaker soil carbon-climate feedbacks resulting from microbial and abiotic interactions. Nature Climate Change 5, 56–60.
Tang, J.Y., Riley, W.J., 2017. SUPECA kinetics for scaling redox reactions in networks of mixed substrates and consumers and an example application to aerobic soil respiration. Geoscientific Model Development 10, 3277–3295.
Tang, J.Y., Riley, W.J., 2019. Competitor and substrate sizes and diffusion together define enzymatic depolymerization and microbial substrate uptake rates. Soil Biology and Biochemistry 139.
Tolla, C., Kooijman, S.A.L.M., Poggiale, J.C., 2007. A kinetic inhibition mechanism for maintenance. Journal of Theoretical Biology 244, 576–587.
van Bodegom, P., 2007. Microbial maintenance: a critical review on its quantification. Microbial Ecology 53, 513–523.
Vasilescu, C., Olteanu, M., Flondor, P., Calin, G.A., 2013. Fractal-like kinetics of intracellular enzymatic reactions: a chemical framework of endotoxin tolerance and a possible non-specific contribution of macromolecular crowding to cross-tolerance. Theoretical Biology and Medical Modelling 10.
Vikstrom, K., Wikner, J., 2019. Importance of bacterial maintenance respiration in a subarctic estuary: a proof of concept from the field. Microbial Ecology 77, 574–586.
Vrugt, J.A., 2016. Markov chain Monte Carlo simulation using the DREAM software package: theory, concepts, and MATLAB implementation. Environmental Modelling & Software 75, 273–316.
Wang, B., Allison, S.D., 2019. Emergent properties of organic matter decomposition by soil enzymes. Soil Biology and Biochemistry 136.
Wang, G.S., Post, W.M., 2012. A theoretical reassessment of microbial maintenance and implications for microbial ecology modeling. FEMS Microbiology Ecology 81, 610–617.
Wilmoth, J.L., Doak, P.W., Timm, A., Halsted, M., Anderson, J.D., Ginovart, M., Prats, C., Portell, X., Retterer, S.T., Fuentes-Cabrera, M., 2018. A microfluidics and agent -based modeling framework for investigating spatial organization in bacterial colonies: the case of pseudomonas aeruginosa and H1-type VI secretion interactions. Frontiers in Microbiology 9.
Zeng, H., Yang, A.D., 2020. Bridging substrate intake kinetics and bacterial growth phenotypes with flux balance analysis incorporating proteome allocation. Scientific Reports 10.
Zhao, W.L., Gentine, P., Reichstein, M., Zhang, Y., Zhou, S., Wen, Y.Q., Lin, C.J., Li, X., Qiu, G.Y., 2019. Physics-Constrained machine learning of evapotranspiration. Geophysical Research Letters 46, 14496–14507.
Zhu, Q., Riley, W.J., Tang, J., Koven, C.D., 2016. Multiple soil nutrient competition between plants, microbes, and mineral surfaces: model development, parameterization, and example applications in several tropical forests. Biogeosciences 13, 341–363.
Zhu, Q., Riley, W.J., Tang, J.Y., Collier, N., Hoffman, F.M., Yang, X.J., Bisht, G., 2019a. Representing nitrogen, phosphorus, and carbon interactions in the E3SM land model: development and dlobal benchmarking. Journal of Advances in Modeling Earth Systems 11, 2238–2258.
Zhu, Y.H., Zabaras, N., Koutsourelakis, P.S., Perdikaris, P., 2019b. Physics-constrained deep learning for high-dimensional surrogate modeling and uncertainty quantification without labeled data. Journal of Computational Physics 394, 56–81.